International Journal of Coal Geology 263 (2022) 104119

Contents lists available at ScienceDirect

International Journal of Coal Geology

journal homepage: www.elsevier.com/locate/coal

Impact of natural weathering on source rocks: Organic and inorganic geochemical evidence from the Triassic Chang 7 outcrop profile in Tongchuan of the Southern Ordos Basin (China)

Shubiao Pan [a,b,c], Yuhong Liao [a,b,*], Bin Jiang [a,b], Zhixiong Wan [a,b,c], Fu Wang [a,b,c]

[a] Key laboratory of Organic Geochemistry, Guangzhou Institute of Geochemistry, Chinese Academy of Sciences, Guangzhou 510640, China
[b] CAS Center for Excellence in Deep Earth Science, Guangzhou 510640, China
[c] University of Chinese Academy of Sciences, Beijing 100049, China

ARTICLE INFO

Keywords:
Weathering
Source rocks
Elemental geochemistry
Organic geochemistry
Palaeoenvironmental proxies

ABSTRACT

Exposure of buried source rocks at or near the surface causes organic matter (OM) to be subjected to loss through weathering impacts. A detailed organic and inorganic investigation of the natural weathering of the Triassic Chang 7 Yishicun Profile in Tongchuan City of the Ordos Basin revealed pronounced changes in bulk, molecular, mineral, and elemental compositions. In this study, systematic and visible variations caused by natural weathering were shown in the amount and composition of both organic (kerogen and extractable organic matter [EOM]) and inorganic matter (minerals and elements). The results indicate that natural weathering could substantially affect the characteristics of source rocks at a depth of 2 m from the surface, resulting in a 41% decrease in total organic carbon (TOC) and a 75% loss of EOM. Furthermore, changes were noted in kerogen elemental compositions, fractional compositions of EOM, and some geochemical parameters from Rock-Eval pyrolysis. The mineral and major, trace, and rare earth element (REE) compositions of the outcrop samples were also analysed and compared. The weathering of source rocks was mainly due to the influence of surface water leaching and biodegradation of the OM. This resulted in the oxidation of kerogen and the preferential depletion of low-carbon-number *n*-alkanes and low-molecular-weight high-water-solubility biomarkers. This has led to bias in petroleum geochemical interpretation based on these organic geochemical parameters. The major elemental composition indicated that the outcrop profile was moderately weathered. Moreover, some commonly used palaeoenvironmental geochemical proxies, including U/Th, AU, Mo, Sr/Ba, Sr/Cu, and P/Ti, display varying degrees of weathering-related alteration. However, other palaeoenvironmental proxies such as V/(V + Ni), Ni/Co, V/Cr, δU, and Ce_{anom} experienced little variation and remained reliable for environmental interpretation. Thus, petroleum resource evaluation and sedimentary environmental analysis of source rocks based on outcrop samples should consider the effects of natural weathering.

1. Introduction

In earth sciences, weathering is the process by which rocks or minerals at or near the surface of the earth are affected by the atmosphere, water, and organisms, resulting in various physical, chemical, and biochemical changes (Petsch et al., 2000, 2001, 2005; Cockell et al., 2011). Weathering of organic matter (OM) plays an important role in the geochemical carbon cycle. The oxidation of OM rocks during weathering

Abbreviations: OM, organic matter; EOM, extractable organic matter; REEs, rare earth elements; DCM, dichloromethane; GC–MS, gas chromatography–mass spectrometry; EI, electron ionisation; SIM, selective-ion monitoring; TIC, total ion current; CV, coefficient of variation; HI, hydrogen index; OI, oxygen index; CN, carbon number; SCh, short chain; LCh, long chain; IS, internal standard; TS/TH, total sterane to total hopane ratio; PAHs, polycyclic aromatic hydrocarbons; MPI, methylphenanthrene index; TAS, triaromatic steroid; XRD, X-ray diffraction; LILE, large-ion lithophile element; TE, transitional element; HFSE, high-field-strength element; LREEs, light rare earth elements; MREEs, middle rare earth elements; HREEs, heavy rare earth elements; NASC, North American shales; CIA, chemical index of alteration; CIW, chemical index of weathering; PIA, plagioclase index of alteration; PAAS, post-Archean Australian Shale; UCC, Upper Continental Crust.

* Corresponding author at: Key laboratory of Organic Geochemistry, Guangzhou Institute of Geochemistry, Chinese Academy of Sciences, Guangzhou 510640, China.
E-mail address: liaoyh@gig.ac.cn (Y. Liao).

https://doi.org/10.1016/j.coal.2022.104119
Received 8 May 2022; Received in revised form 17 August 2022; Accepted 6 October 2022
Available online 13 October 2022
0166-5162/© 2022 Elsevier B.V. All rights reserved.

provides important controls on the O_2 and CO_2 concentrations in the Earth's atmosphere over geologic time (Petsch et al., 2000; Frings and Buss, 2019). Exposure of buried source rocks at or near the surface because of tectonic uplift causes OM in them to be subjected to loss through surface-water dissolution, erosion, oxidation, and biological assimilation. In the early stages of hydrocarbon exploration and development, drilling and coring of source rocks were limited, and many exploration surveys were based on outcrop samples. Currently, China's oil and gas exploration has developed toward deep and ultra-deep strata (Dai et al., 2018; Li et al., 2021), and the cost of drilling and coring at greater depths is high. Rock chip sampling is affected by drilling-fluid contamination (Carvajal-Ortiz and Gentzis, 2015). Therefore, research on the changes in geochemical characteristics of source rocks during weathering is of crucial theoretical and practical significance for the elucidation of the weathering process in source rocks, exploration of effective evaluation indicators based on outcrop samples, and prediction of the hydrocarbon potential of source rocks in the basin using outcrop data (Littke et al., 1991; Marynowski et al., 2011a; Marynowski et al., 2011b; Tang et al., 2018).

Previous studies have primarily considered the loss of organic carbon, general variation in the composition of kerogen (Leythaeuser, 1973; Petsch et al., 2001) and variations in the molecular composition of extractable OM (EOM) (Clayton and King, 1987; Littke et al., 1991; Petsch et al., 2000; Marynowski et al., 2011a, 2011b; Tamamura et al., 2015). These changes are revealed as substantial losses in the amount of OM, selective leaching of kerogen macromolecules, and variations in the concentration and distribution of EOM due to oxidation. Many studies have shown that the interpretation of biomarkers as palaeoenvironmental indicators, OM source indicators, and thermal evolutionary stages can be substantially influenced by weathering processes (Clayton and King, 1987; Petsch et al., 2000; Marynowski et al., 2011a, 2011b). However, although these variations are visible in most weathering profiles reported in previous studies, weathering-induced alterations can vary from one weathering profile to another due to the different degree of weathering, which is determined by a combination of many factors. They can be attributed to intrinsic factors such as mineral composition, porosity, and permeability of the source rock; type and maturity of OM (Spears and Taylor, 1972; Leythaeuser, 1973; Clayton and Swetland, 1978; Tao et al., 2016) and extrinsic factors such as climate, exposure time, and microbial activity (Petsch et al., 2005; Fischer et al., 2009; Marynowski et al., 2011a; Tao et al., 2016; Frings and Buss, 2019).

The variation in the composition of major and trace elements (including rare earth elements [REEs]) in shale caused by weathering has been relatively poorly reported. Peucker-Ehrenbrink and Hannigan (2000) discussed the mobility of rhenium and platinum group elements during weathering of organic-rich deposits, and Kolowith and Berner (2002) studied the effect of weathering on phosphorus concentrations. Ma et al. (2011) and Jin et al. (2017) have discussed the mobility and fractionation of REEs during shale weathering. Marynowski et al. (2017) and Tang et al. (2018) reported element concentrations and palaeoenvironmental proxies of black shales during weathering. Nevertheless, the behaviour of many other elements remains poorly understood. Thus, interpretations of palaeoenvironmental conditions based on conventional elemental indicators may be influenced by weathering.

This study was novel in its approach to avoid strong vertical inhomogeneities in shale composition and its focus on progressive changes in rock composition because of weathering. To avoid strong vertical inhomogeneities in the mineral and elemental composition of the shale (Fathi and Akkutlu, 2009; Fan et al., 2012; Chen et al., 2015), samples were collected along a single horizontal stratum from Triassic Yanchang Formation source rocks in the Yishicun Profile of the Ordos Basin. We focused on progressive changes in the mineralogical composition and bulk and molecular compositions of sedimentary OM. In addition, we documented the variations in major and trace element abundances, with special attention to the disturbance of key palaeoenvironmental proxies. Finally, petrogeochemical interpretations and palaeoenvironment determination based on these organic and inorganic geochemical evidence during weathering are discussed and valid geochemical indicators are identified.

2. Geological setting

The Ordos Basin, located in the western part of the North China Craton, is a large Mesozoic inland depressional lake basin superimposed on the early and late Palaeozoic North China Craton Basin (Fig. 1A). It covers an area of 25×10^4 km^2 and is a large superimposed sedimentary basin that experienced stable subsidence in the early stages and migration of the depressional centre in the later stages, forming a large depression lacustrine deposit in the Late Triassic Yanchang Formation. According to sedimentary cycles and lithological associations, the Yanchang Formation (T_3y) is divided into 10 subunits, ranging from 1 to 10 from top to bottom (Fig. 1B; Li et al., 2016).

The Yishicun Profile is in Tongchuan city within the Weibei uplift tectonic unit (Fig. 1C). Because of tectonic extrusion and uplift in the Yanshan–Himalayan orogenic period, the Yanchang Formation in this area is widely exposed at the surface (Song et al., 2019). In this study, samples were collected from the Yishicun Profile (a recently exposed roadcut), which is located 5 km southwest of Yaoqu Town. The Chang 7_3 and Chang 7_2 subsections are exposed in this profile, and the occurrence of black oil shale is nearly horizontal. The lithology of this profile is composed of oil shale and mudstone with thin tuff intercalations (Fig. 1C).

According to the climate data from the study area over the last three decades, the Tongchuan city is well-lit with 2250.7–2387.7 h of mean annual sunshine duration. The temperature varies widely from day to night with an annual average temperature of 9.7–12.7 °C. The Yishicun Profile is in the mountainous area, which has sufficient precipitation with an average annual precipitation of ~700 mm. There are numerous waterfalls and streams throughout the mountains, which are steep with an altitude of 1500 m. Additionally, the flora and trees in the area grow densely because of a warm and humid climate, and the surface erosion is quite severe.

3. Samples and methods

3.1. Samples

Ten samples (black oil shale) of approximately 500 g each were obtained from the Yishicun Profile along the roadcut (Fig. 1A). Sample locations (black dots) were spaced at intervals of 0.5–1 m along a single stratigraphic horizon. The samples were collected by drilling horizontally into the outcrop along this single exposed layer to avoid interlayer heterogeneity in lithology and OM content (Fig. 1C). The shale samples were obtained at 20–30 cm into the face of the outcrop rather than directly from the exposed surface layer to ensure that the degree of surface weathering of the collected samples was consistent. Fresh rock samples were collected and stored in plastic bags to ensure minimal contamination pending experimental analysis. To analyse the degree of weathering of the samples intuitively and conveniently, their positions were directly converted into the vertical distance below the soil/vegetation layer (Fig. 1C, red line) to the sampling horizon (blue line), depicted by the lengths of the yellow lines in Fig. 1C. The suite of samples could be divided into three stages according to the horizontal distance from the samples to the surface soil/vegetation cover. The weathering of samples generally increased from Stage I to Stage III, as evidenced by a colour change from black to brown and an increase in rock fissility and friability. Table 1 shows the sample numbers and depths of the source rock samples.

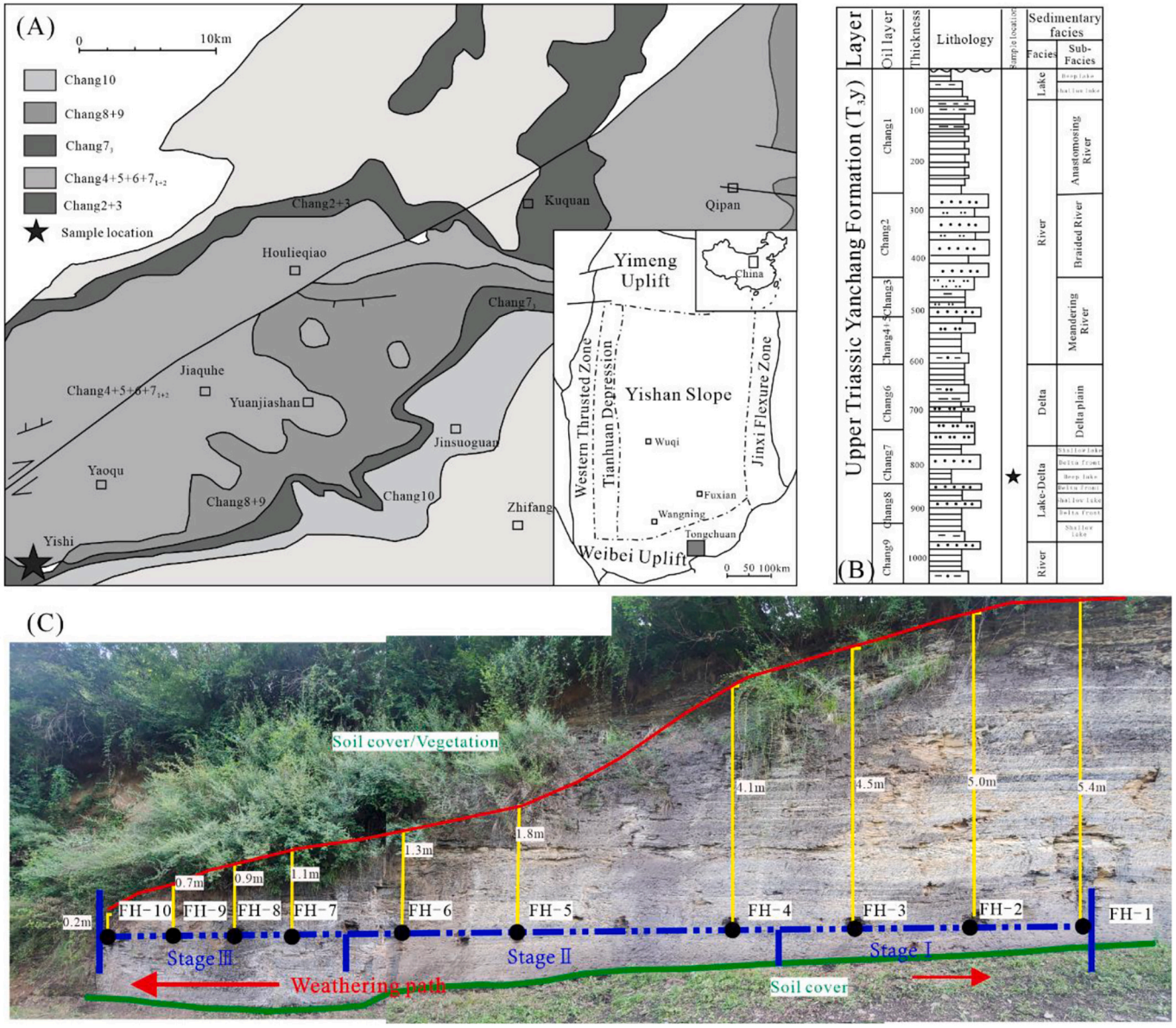

Fig. 1. (A) Tectonic map of Ordos Basin showing the location of the studied section (modified after Song et al., 2019); (B) stratigraphic column of the Upper Triassic Yanchang Formation (modified after Li et al., 2017); (C) outcrop profile with numbers denoting the samples collected through the Upper Triassic Yanchang Formation in the Tongchuan area.

3.2. Methods

All outcrop samples were crushed to approximately 100 mesh and then dried in an oven for 10 h at 60 °C (176 °F) before geochemical analyses. The partially powdered samples were used for mineral composition analysis using an X-ray diffractometer (Olympus Innova-X BTX-II). The diffractometer was equipped with a Co X-ray tube operating at 31 kV and 0.4 mA. The exposure time was 70 min, and the exposure rate was three times per minute (Zheng et al., 2018). The relative mineral percentages were estimated semi-quantitatively using the area under the curve for the major peaks of each mineral, which was implemented using the relevant software (XPowder, Ver. 2010).

After approximately 200 mesh powdered samples were digested with perchloric acid, nitric acid, hydrofluoric acid, and hydrochloric acid, the volume was fixed with dilute hydrochloric acid. Inductively coupled plasma emission spectroscopy (Agilent 5110) was used to measure the trace elements and inductively coupled plasma mass spectrometry (Agilent 7900) was employed to measure the REEs and major elements.

TOC analysis of all samples was performed using a LECO CS230 carbon-sulfur analyser. Inorganic carbon in the samples was removed using dilute hydrochloric acid (5% HCl). These samples were burned in an oxygen-rich carrier gas at 900 °C to convert the organic carbon into carbon dioxide. The basic parameters were obtained using a Rock-Eval 6 instrument. The initial temperature of the pyrolysis oven was set at 300 °C with a holding time of 3 min. Then the temperature was programmed to increase to 650 °C at a rate of 25 °C/min using nitrogen as the carrier gas.

The extracts (bitumen) were prepared using approximately 50 g of clean and powdered aliquots of each rock sample. The extract was extracted for 72 h in a Soxhlet apparatus with dichloromethane (DCM): methanol (93:7, v:v). Activated copper foil was added to remove elemental sulfur from the extracts. The extracts were separated into maltene and asphaltene fractions using a de-asphaltening procedure, as described in detail by Liao et al. (2009). The maltene fraction was fractionated into saturated, aromatic, and resin fractions by silica gel/alumina column chromatography and eluted with n-hexane, DCM/n-

Table 1
Partial general geochemical indicators of the Triassic Yanchang Formation source rocks from the Yishicun Profile in the Tongchuan area, Ordos Basin.

S No.	Depth (m)	TOC (%)	S1 + S2 (mg/g)	S2/ TOC	HI	OI	S1 (mg/g)	S2 (mg/g)	T_{max} (°C)	'A' (mg/g)	Sat %	Aro %	Res %	Asp %	Sat/ Aro	N %	O %	C %	H %	H/C	O/C	N/C
FH-1	5.45	24.91	84.52	3.25	325.00	37.00	3.64	80.88	431	11.18	30.24	4.08	39.11	26.57	7.41	4.03	78.35	6.95	12.03	1.06	0.12	0.04
FH-2	4.95	24.01	81.48	3.24	324.00	34.00	3.74	77.74	431	11.92	33.44	6.32	37.97	22.27	5.29	3.63	78.24	6.76	11.36	1.04	0.11	0.04
FH-3	4.48	24.46	79.59	3.08	308.00	35.00	4.17	75.42	431	13.91	34.90	4.14	40.45	20.51	8.43	3.50	79.55	6.86	12.48	1.04	0.12	0.04
FH-4	4.08	17.70	55.74	3.04	304.00	42.00	1.96	53.78	431	8.84	29.67	3.56	44.86	21.91	8.33	2.92	66.76	5.65	12.49	1.02	0.14	0.04
FH-5	1.81	20.26	53.98	2.58	258.00	45.00	1.76	52.22	431	6.13	30.45	2.85	45.41	21.29	10.68	3.14	66.84	5.64	15.75	1.01	0.18	0.04
FH-6	1.33	19.88	53.68	2.63	263.00	51.00	1.39	52.29	431	5.42	19.82	2.59	41.22	36.37	7.65	3.28	71.41	6.22	19.30	1.05	0.20	0.04
FH-7	1.12	20.12	56.61	2.74	274.00	45.00	1.55	55.06	433	4.04	21.22	2.59	43.21	32.98	8.19	3.08	67.88	5.35	14.07	0.95	0.16	0.04
FH-8	0.91	17.67	48.60	2.70	270.00	51.00	0.89	47.71	435	3.74	29.03	2.36	38.33	30.28	12.30	3.17	71.03	5.81	17.55	0.98	0.19	0.04
FH-9	0.70	16.13	40.78	2.48	248.00	43.00	0.83	39.95	434	3.26	19.97	1.20	44.95	33.88	16.64	3.01	65.88	5.44	15.09	0.99	0.17	0.04
FH-10	0.20	14.44	30.01	2.05	205.00	51.00	0.42	29.59	432	3.12	15.81	1.01	45.41	37.77	15.65	3.26	68.65	5.64	22.45	0.99	0.25	0.04
Mean		19.96	58.50	2.78	278	43	2.04	56.46	432	7.16	26.46	3.07	42.09	28.38	10.06	3.30	71.46	6.03	15.26	1.01	0.16	0.04
CV (%)		18.05	30.84	13.59	14	15	65.82	29.66	0.35	55.92	25.02	50.60	7.20	23.54	37.00	10.16	7.44	10.22	23.54	3.53	26.80	4.83

Sat: saturated fraction; Aro: aromatic fraction; Res: resin; Asp: asphaltene.

hexane (3:1, v:v), and DCM/methanol (2:1, v:v). An appropriate quantity of $C_{24}D_{50}$ was added to the saturated fraction as an internal standard to quantify *n*-alkanes concentrations. Solvent-insoluble OM (kerogen) was obtained by successive HCl/HCl:HF/HCl digestion of powdered samples after extraction through a demineralising procedure (Goklen et al., 1984).

GC–MS analyses of the saturated and aromatic fractions were performed with an Agilent 8890/5977MSD instrument equipped with an HP-1MS fused silica column (60 m × 0.32 mm i.d. × 0.25 μm film thickness). Appropriate amounts of 20R-5α(H),14α(H),17α(H)-[2,2,4,4-d4] cholestane and phenanthrene-d10 were added to the saturated and aromatic hydrocarbons as internal standards for the quantification of biomarkers. Helium (purity 99.999%) was introduced as the carrier gas at a flow rate of 1.2 mL/min. The temperature of injection port was 285 °C and pulse split injection was performed. Simultaneously, the GC oven was programmed to hold at 60 °C for 2 min, then increase to 290 °C at a rate of 4 °C/min with a final holding at 290 °C for 20 min. The mass spectrometer was operated in the electron ionisation (EI) mode at a voltage of 70 eV. The ion source was maintained at 260 °C. The MS was operated in both full-scan mode (*m/z* 50–650) and selective-ion monitoring (SIM) mode. The data of the biomarkers were acquired in SIM mode for the total ion current (TIC).

The elemental analysis (CNS/O) of the kerogen concentrates was performed using an Elementar Vario EL III elemental analysis system. The accuracy of the data was monitored using standards of known isotopic composition (C: 65.43%; H: 6.70%; N: 8.47%; and O: 19.40%), with normalisation of the weight percentages of these elements. All analytical experiments in this study were performed at the Organic Laboratory of the Guangzhou Institute of Geochemistry, Chinese Academy of Sciences.

4. Results

In this study, the coefficient of variation (CV), which is the percentage of the standard deviation of the original data to the mean of the original data, was used to characterise the degree of dispersion of the measured data in the sample suite. It is necessary to eliminate the influence of different measurement scales and dimensions during the organic and inorganic instrumental analyses. Therefore, the magnitude of variability in geochemical parameters can be compared using CV to determine the effect of weathering on the samples. The higher the CV of the parameter, the greater its variability, indicating that the weathering effect had a more pronounced influence.

4.1. General geochemical characteristics

4.1.1. Total organic carbon content and rock-eval analysis

The results of the TOC and Rock-Eval analyses are presented in Table 1 (Fig. 2). The TOC content of these samples ranged from 14.44% to 24.91% (mean = 19.96%, CV =18.05%), which shows a smooth and gradual decrease toward the top interval of the profile. The Rock-Eval S1 + S2 values ranged from 30.01 to 84.52 mg HC/g rock (mean = 58.50 mg HC/g rock, CV = 30.84%), which showed the same trend with depth as did TOC (Fig. 2). The hydrogen index (HI) was in the range of 205–325 mg HC/g TOC (mean = 277.9 mg HC/g TOC, CV = 13.59%) and the oxygen index (OI) was in the range of 34–51 mg CO_2/g TOC (mean = 43.40 mg CO_2/g TOC, CV =14.98%). HI and OI have opposite trends with depth. HI gradually increases and OI gradually decreases, as observed in a previous study by Bjorøy and Vigran (1980).

It is notable that parameters such as TOC, S1 + S2 and EOM, which are often used to evaluate the abundance of OM in source rocks, decrease with weathering. The variation in these parameters was evident in Stage III samples that had experienced more severe weathering. These parameters depicted only slight change in Stage I, and some (such as TOC, S1, EOM and OI) showed the opposite trend with depth.

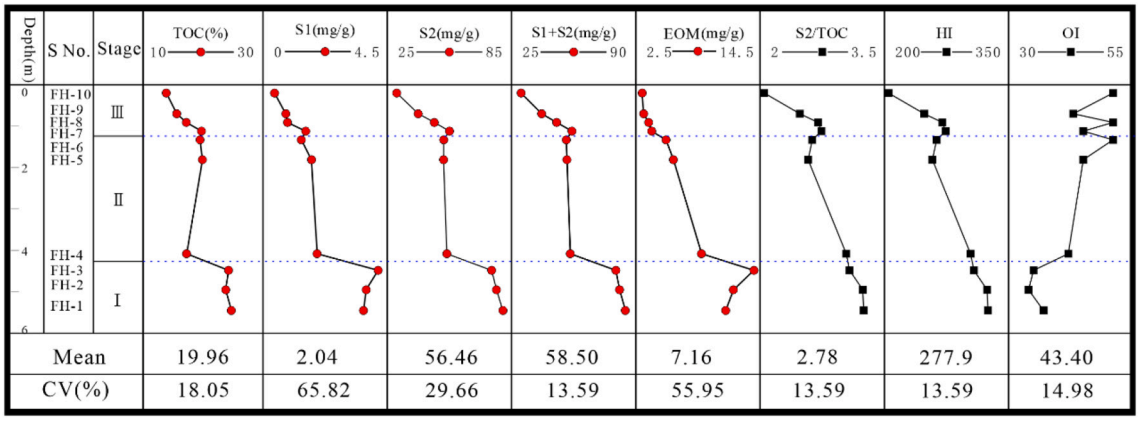

Fig. 2. Abundance indices of OM and their related statistical parameters by Rock-Eval and Soxhlet extracts for FH-series samples from the Yishicun Profile in the Tongchuan area, Ordos Basin.

4.1.2. Bulk composition of EOM

As shown in Table 1 and Fig. 2, the contents of EOM were in the range of 3.12–13.91 mg/g (mean = 7.16 mg/g, CV = 55.92%). The aromatic fraction contents were the lowest in the EOM, while the resin and asphaltene contents were the highest. The saturated and aromatic fractions showed a clear decreasing trend, whereas the resin and asphaltenes showed a relative increasing trend during weathering. The high ratio of saturated to aromatic fractions (Sat/Aro) in Stage III (Fig. 3), accompanying a gradual decrease in EOM content, show the preferential depletion of aromatic hydrocarbons and gradual enrichment of polar fractions in source rocks during weathering.

4.1.3. Kerogen elemental compositions

The elemental composition of kerogen from the source rocks was normalized by the sum of C, H, N, and O. Table 1 shows the elemental composition of the FH-series samples and their statistical parameters. The CV values of O/C (mean = 0.16), H/C (mean = 1.01), and N/C (mean = 0.04) were 26.80%, 3.53%, and 4.83%, respectively, indicate the preferential loss of both carbon and hydrogen, and the relative enrichment of oxygen during weathering. During weathering there is no alteration of nitrogen, but a substantial enrichment of oxygen and a slight depletion of hydrogen compared to carbon in the kerogen. This is consistent with the report by Petsch et al. (2000) based on the kerogen from different weathering profiles.

4.2. Molecular composition

4.2.1. N-alkanes and isoprenoids

The TIC plots of saturated hydrocarbons in the samples are shown in Fig. 4. Analytical data showed that the carbon number (CN) of *n*-alkanes in most samples ranged from *n*-C_{12} to *n*-C_{35}, except for the samples (FH-10, FH-9, and FH-8) in Stage III which had *n*-alkanes CNs ranging from *n*-C_{13} to *n*-C_{35}. Most samples showed a unimodal and low CN *n*-alkane distribution with the main peak at C_{17} and C_{19}, whereas the samples in Stage III showed a high CN *n*-alkane distribution with the major alkanes of C_{29}. In all samples, except for three samples in Stage III, long-chain alkanes (*n*-C_{27}–*n*-C_{29}) were dominant relative to short-chain alkanes (*n*-C_{17}–*n*-C_{19}). Notably, the ratios of short-chain to long-chain alkanes (SCh/LCh) were lower in highly weathered samples (Table 2). This is inconsistent with previous reports, which suggest that the oxidative evolution of *n*-alkanes usually leads to a gradual increase in short-chain alkanes and degradation of long-chain compounds (Faure et al., 1999; Marynowski and Wyszomirski, 2008). Similar trends were observed for the concentration of *n*-alkanes in the outcrop samples. Table 3 demonstrates that the *n*-alkanes total concentrations of samples in Stage III ranged from 10.27 to 12.27 μg/g rock, while the remaining sample concentrations of *n*-alkanes were relatively higher, ranging from 28.87 to 61.76 μg/g rock. The distribution of *n*-alkanes is consistent with other weathering reports that illustrate the preferential loss of lower CN *n*-

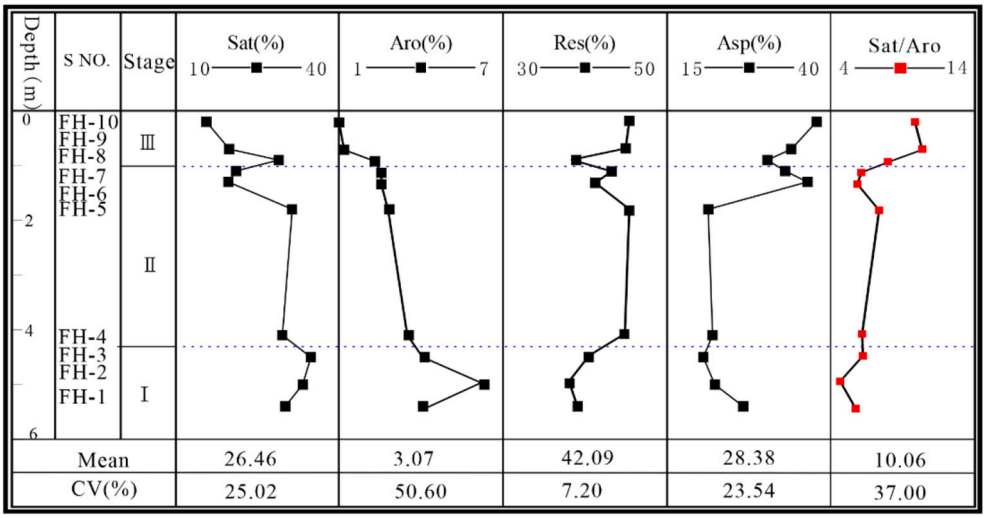

Fig. 3. Relative contents of EOM bulk compositions and their related statistical parameters for the series samples from Yishicun Profile in the Tongchuan area, Ordos Basin.

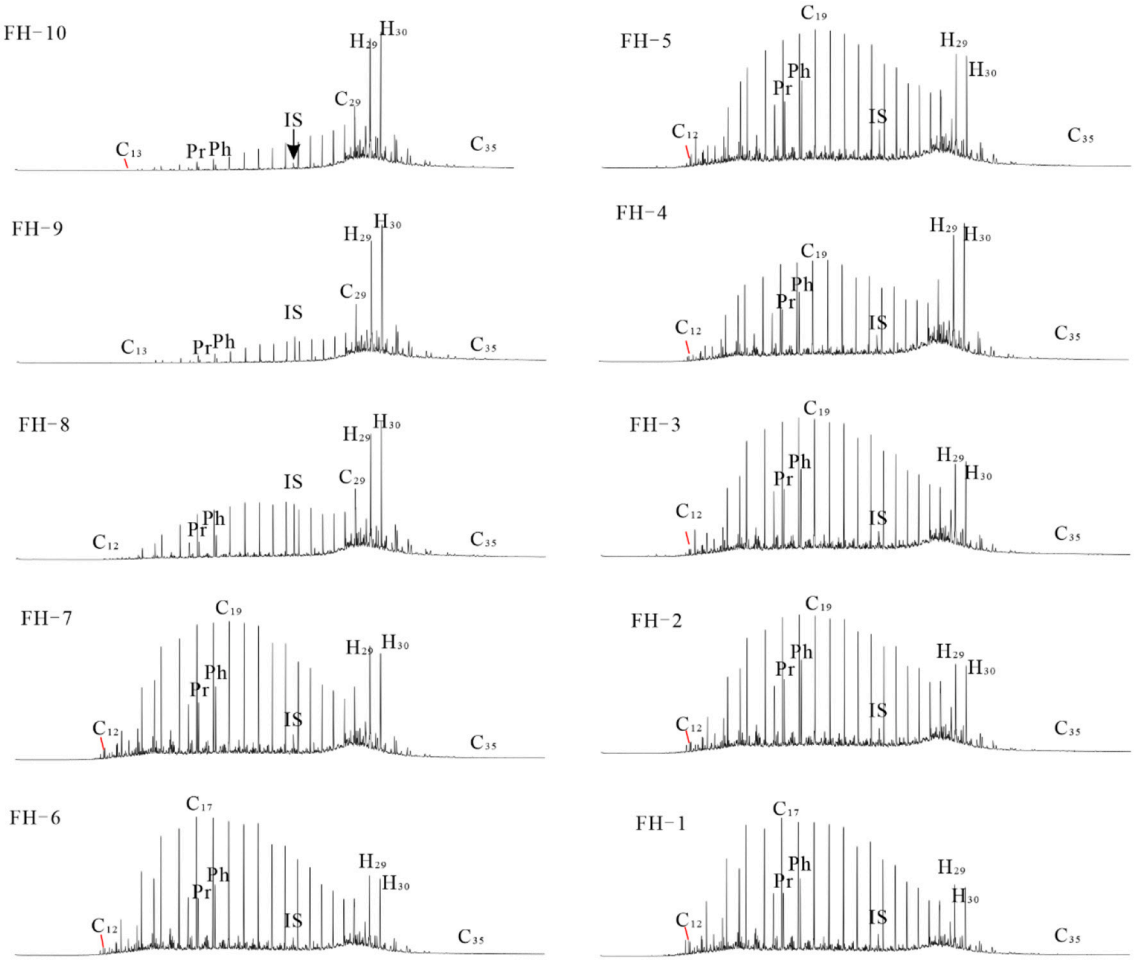

Fig. 4. Total ion chromatograms (TIC) plot of saturated hydrocarbon fractions for the source rock samples from Yishicun Profile in the Tongchuan area, Ordos Basin; IS: internal standard ($C_{24}D_{50}$).

alkanes during weathering (Clayton and Swetland, 1978; Bjorøy and Vigran, 1980; Marynowski et al., 2011a). This may indicate that, in addition to oxidation, the distribution of n-alkanes in the weathered samples was also affected by other factors, such as surface water leaching and evaporation (Palmer, 1993; Skręt et al., 2010).

As shown in Fig. 4 and Table 2, the distributions of isoprenoids in the FH-series samples were stable. The Pr/Ph ratio is in the range of 0.53–0.60 (mean = 0.56, CV = 4.08%), which indicates a strong reducing environment (Peters et al., 2005). Pr/nC_{17} and Ph/nC_{18} values ranged from 0.33 to 0.45 (mean = 0.39, CV = 12%) and from 0.59 to 0.81 (mean = 0.68, CV =14.76%), respectively. The ratio of Pr/Ph to Pr/nC_{17} are almost stable for each sample during weathering, except for a slight decrease in Ph/nC_{18}.

4.2.2. Steranes and terpanes

Pregnane (S_{21}), homopregnane (S_{22}), regular steranes (C_{27}–C_{29}), and diasteranes (C_{27}–C_{29}) were identified on the *m/z* = 217 mass chromatograms (Fig. 5A). The relative contents of C_{27}, C_{28}, and C_{29} regular steranes were approximately 16.93–24.94% (mean = 22.02%, CV = 13.11%), 28.31–31.21% (mean = 30.31%, CV = 3.22%), and 44.85–54.76% (mean = 47.67%, CV =7.22%), respectively. The samples in Stage III showed the distribution of $C_{29} > C_{27} > C_{28}$ and an inverse L-shape on the sterane fragmentograms. The relative content of C_{27}ααα(20R) gradually decreased, and the relative content of C_{29}ααα(20R) gradually increased, indicating that weathering had a pronounced effect on the distribution of C_{27}–C_{29} regular steranes. The C_{27} and C_{29} sterane isomerisation parameters [ααα 20S/(20S + 20R) and αββ/(αββ + ααα)] remained virtually unchanged in all samples across the outcrop profile (Table 2). Interestingly, the C_{21-22} pregnane/C_{27-29} regular steranes and S_{21}/S_{22} ratio for the outcrop samples show a gradual decrease during weathering, which indicates that the distribution of pregnane and homopregnane will be affected by weathering.

The peaks identified in *m/z* 191 mass chromatograms were C_{19}–C_{24} tricyclic terpanes (TT_{19-24}), C_{24} tetracyclic terpanes (TeT_{24}), and C_{27}–C_{35} pentacyclic hopanes (Fig. 5B). The distribution of C_{27}–C_{35} pentacyclic hopanes was stable, with C_{30} αβ hopane being predominant in all samples. Ts (18α(H)-22, 29, 30-trisnorneohopane) and Tm (17α(H)-22, 29, 30-trisnorhopane) are also common pentacyclic terpanes, and their relative ratios are commonly used to indicate OM maturity in source rocks (Peters et al., 2005). In this study, the Ts/(Ts + Tm) ratio remained stable during weathering. The distribution of related tricyclic terpanes was characterised by the order $C_{23} > C_{21} > C_{20}$ for all samples. However, the TT_{21}/TT_{23} and TT_{20}/TT_{23} ratios gradually decreased during weathering (Table 2). Furthermore, the total tricyclic terpene content decreased faster than that of pentacyclic terpanes, resulting in a gradual decrease in the total tricyclic terpenes/C_{30} hopane ratio (TT/H_{30}).

It is notable that the steranes and terpenes changed differently. In this study, the ratio of C_{29}-ααα 20R sterane to 17α(H)-hopane (C_{29}/ H_{30}, CV = 14.83%) and the total sterane to total hopane ratio (TS/TH, CV = 27.39%) decreased during weathering. This indicates that hopane compounds are more resistant to weathering than sterane compounds. This is consistent with the order of resistance to biodegradation of components in crude oil (Seifert and Moldowan, 1979; Volkman et al.,

Table 2
Molecular parameters based on biomarker and PAH distributions of the Upper Triassic Yanchang Formation source rocks from the Yishicun Profile in the Tongchuan area, Ordos Basin.

Biomarker ratios	Stage I			Stage II				Stage III			Mean	CV (%)
	FH-1	FH-2	FH-3	FH-4	FH-5	FH-6	FH-7	FH-8	FH-9	FH-10		
n-alkanes												
CPI	1.14	1.13	1.12	1.14	1.12	1.14	1.13	1.1	1.11	1.1	1.12	1.4
OEP	1.06	1.03	1.05	1.04	1.05	1.07	1.03	1.05	1.08	1.09	1.06	1.91
Major Alkanes	17	19	19	19	19	17	19	29	29	29		
SCh/LCh	2.3	1.86	1.97	1.92	1.9	2.38	2.28	1.21	0.43	0.32	1.66	45.36
C_{21}-/C_{22}+	1.44	1.14	1.17	1.07	1.06	1.44	1.26	0.61	0.22	0.2	0.96	47.77
Pr/Ph	0.59	0.56	0.57	0.54	0.56	0.60	0.56	0.54	0.54	0.53	0.56	4.08
Pr/nC_{17}	0.38	0.45	0.4	0.45	0.44	0.33	0.34	0.34	0.38	0.36	0.39	12
Ph/nC_{18}	0.66	0.81	0.73	0.83	0.77	0.57	0.6	0.6	0.6	0.59	0.68	14.76
TAR	0.34	0.45	0.41	0.49	0.47	0.32	0.38	0.92	3.52	4.06	1.14	124.52
Steranes												
ααα20R C_{27}/(C_{27} + C_{28} + C_{29})	24.94	23.94	23.73	22.68	23.7	24.18	23.06	18.93	18.09	16.93	22.02	13.11
ααα20R C_{28}/(C_{27} + C_{28} + C_{29})	30.16	31.21	31.18	30.8	30.81	30.78	30.53	28.83	30.52	28.31	30.31	3.22
ααα20R C_{29}/(C_{27} + C_{28} + C_{29})	44.9	44.85	45.09	46.51	45.49	45.04	46.42	52.24	51.4	54.76	47.67	7.72
S_{21}/S_{22}	1.4	1.3	1.45	1.42	1.33	1.28	1.23	1.24	1.02	1.13	1.28	10.42
S_{21-22}/C_{27-29}	0.18	0.14	0.13	0.11	0.13	0.16	0.13	0.08	0.03	0.04	0.11	43.36
C_{27}ααα20S/(20S + 20R)	0.53	0.53	0.53	0.54	0.53	0.53	0.55	0.53	0.51	0.52	0.53	1.99
C_{29}ααα20S/(20S + 20R)	0.43	0.43	0.44	0.45	0.43	0.43	0.43	0.39	0.42	0.38	0.42	5.11
C_{27}αββ/(αββ + ααα)	0.34	0.37	0.37	0.37	0.36	0.36	0.36	0.35	0.34	0.31	0.35	5.35
C_{29}αββ/(αββ + ααα)	0.37	0.39	0.39	0.38	0.38	0.38	0.38	0.36	0.37	0.33	0.37	4.74
C_{29}/H_{30}	0.07	0.08	0.08	0.07	0.08	0.07	0.07	0.06	0.05	0.05	0.07	14.83
TS/TH	0.18	0.25	0.26	0.2	0.24	0.22	0.21	0.15	0.12	0.11	0.19	27.39
Terpanes												
Ts/(Ts + Tm)	0.21	0.21	0.18	0.22	0.2	0.21	0.22	0.2	0.19	0.19	0.2	6.59
H_{29}/H_{30}	0.71	0.7	0.7	0.72	0.67	0.76	0.74	0.65	0.61	0.64	0.69	6.8
TT_{23}/(TT_{23} + TT_{24})	0.7	0.69	0.68	0.68	0.69	0.69	0.72	0.7	0.68	0.68	0.69	1.86
C_{31}22S/(22S + 22R)	0.56	0.57	0.57	0.56	0.56	0.57	0.55	0.56	0.55	0.55	0.56	1.46
C_{32}22S/(22S + 22R)	0.61	0.53	0.6	0.6	0.6	0.54	0.58	0.59	0.62	0.6	0.59	5.02
TT/H_{30}	0.26	0.26	0.25	0.21	0.26	0.28	0.24	0.1	0.04	0.04	0.19	49.27
TT_{21}/TT_{23}	0.93	0.9	0.89	0.8	0.89	0.91	0.89	0.81	0.65	0.66	0.83	12.31
TT_{20}/TT_{23}	0.71	0.65	0.65	0.57	0.65	0.69	0.62	0.55	0.36	0.39	0.58	20.63
TT_{23}/H_{30}	0.07	0.07	0.07	0.06	0.07	0.07	0.06	0.03	0.01	0.01	0.05	48.65
Aromatic hydrocarbon												
P/ΣMP	0.35	0.49	0.58	0.58	0.89	0.85	0.74	0.97	0.93	0.87	0.72	29.09
MPI-R	0.61	0.62	0.65	0.5	0.71	0.69	0.66	0.72	0.67	0.67	0.65	9.66
MPI1	0.58	0.52	0.5	0.4	0.42	0.42	0.44	0.41	0.39	0.41	0.45	13.72
TAS(C_{20-21})/(C_{26-28})	0.09	0.11	0.11	0.09	0.13	0.14	0.06	0.06	0.04	0.05	0.09	41.01
TAS_{20}/TAS_{21}	0.97	0.95	0.95	0.99	0.98	0.97	0.86	0.92	0.74	0.75	0.91	10.4
DBT/P	0.1	0.15	0.11	0.05	0.02	0.03	0.02	0.01	0.04	0.01	0.05	89.25

CPI = Carbon Preference Index [Σ(C_{25-33})odd/Σ(C_{24-32})even + Σ(C_{25-33})odd/Σ(C_{26-34})]/2 (Bray and Evans, 1961); OEP = Odd-over-Even Predominance: [(C_i + 6 × C_{i+2} + C_{i+4})/(4 × C_{i+1} + 4 × C_{i+3})]^m, m=$(-1)^{i+1}$; i + 2 denotes the main peak CN of *n*-alkanes, (Scalan and Smith, 1970); SCh/LCh = short chain to long chain *n*-alkanes ratio: (nC_{17} + nC_{18} + nC_{19})/(nC_{27} + nC_{28} + nC_{29}); Pr/Ph = Pristane/Phytane; TAR = The terrigenous to aquatic ratio: (C_{27} + C_{29} + C_{31})/(C_{15} + C_{17} + C_{19}), (Bourbonniere and Meyers, 1996); S_{21}/S_{22} = pregnane/homopregnane; S_{21-22}/C_{27-29} = S_{21-22} pregnane/C_{27-29} regular steranes; C_{29}/H_{30} = C_{29} ααα 20R sterane/17α(H)-hopane; TS/TH = total steranes/total hopanes: C_{27-29} ααα(20S + 20R) and αββ(20S + 20R) regular steranes/C_{29}–33 17α-hopanes (including 22S and 22R epimers); H_{29}/H_{30} = C_{29}-17α(H)-norhopane to C_{30}-17α(H)-hopane ratio; TT/H_{30} = tricyclic terpanes/17α(H)-hopane; P/ΣMP = P/(1-MP + 4-MP + 9-MP + 2-MP + 3-MP); MPI1 = 1.5(2-MP + 3-MP)/(Ph + 1-MP + 9-MP), (Radke and Welte, 1983), MPI-R = (3-MP + 2-MP)/(9-MP + 1-MP), (Cassani et al., 1988).

1983; Peters and Moldowan, 1993) and the study of palaeoweathering in black shale by Marynowski et al. (2011a).

4.2.3. Aromatic hydrocarbon biomarker

The concentration of most PAHs decreases during weathering, as shown on Table 4. Table 2 shows the commonly used aromatic maturity parameters: the methylphenanthrene index (MPI-R, MPI1) and the ratio of short sidechain triaromatic steroid hydrocarbons (TAS) to long sidechain TAS [TAS(C_{20-21})/(C_{26-28})]. MPI-R (CV = 9.66) and MPI1 (CV = 13.72) showed a slight increasing trend with weathering, and P/ΣMP (CV = 29.09%) gradually increased, which is consistent with a previous study of weathering (Marynowski et al., 2011a). However, TAS(C_{20-21})/(C_{26-28}) exhibited a noticeable tendency to decrease during weathering, which is consistent with the tendency of the S_{21-22}/C_{27-29} steranes during weathering. Interestingly, DBT/P (CV = 89.25%), an indicator of water washing (Palmer, 1984; Lafargue and Barker, 1988; Alkhafaji, 2021), decreased sharply in Stage III and showed a pronounced decreasing trend during weathering.

4.3. Inorganic geochemical characteristics

4.3.1. Mineralogical characteristics

The outcrop samples were characterised by quartz, albite, potassium feldspar, carbonate minerals (calcite and dolomite), pyrite, and clay minerals (illite and montmorillonite) based on X-ray diffraction (XRD) analysis (Fig. 6A and Table S1), indicating a lithology of carbonaceous mudstone. Carbonate minerals were the most variable of all mineral compositions during weathering, followed by pyrite and feldspar minerals. In Stage III, the carbonate minerals and pyrite were heavily depleted. It is notable that in Stage I, the carbonate minerals and pyrite clearly follow opposite trends, which is consistent with the results of the organic geochemical characteristics above.

4.3.2. Major elements

As shown in Table S2, SiO_2 is the main chemical composition among all the FH-series samples, ranging from 36.85% to 43.33%. The MnO content was the lowest and was too low to be detected. CaO (0.55–1.55%, average = 1.15%) and Fe_2O_3 (10.34–13.94%, average = 11.7%) were the most variable of all major elements, with CVs of

Table 3
Concentrations (μg/g rock) of *n-alkanes* with different CNs in the source rock samples from Yishicun Profile.

	Stage I			Stage II				Stage III		
	FH-1	FH-2	FH-3	FH-4	FH-5	FH-6	FH-7	FH-8	FH-9	FH-10
C_{12}	0.93	0.40	0.14	0.11	0.16	0.18	0.11			
C_{13}	2.73	1.35	0.87	0.88	0.69	1.04	0.74	0.06	0.00	0.01
C_{14}	4.43	2.71	2.54	2.19	1.81	2.27	1.54	0.25	0.04	0.06
C_{15}	5.81	4.07	4.43	3.57	2.98	3.14	2.26	0.55	0.16	0.16
C_{16}	5.03	3.73	4.10	3.51	3.14	3.07	2.34	0.66	0.20	0.20
C_{17}	5.27	4.41	4.49	3.74	3.61	3.44	2.66	0.86	0.31	0.28
C_{18}	4.81	3.86	4.19	3.55	3.40	3.06	2.42	0.81	0.36	0.31
C_{19}	4.84	4.03	4.17	3.79	3.63	3.06	2.43	0.92	0.47	0.39
C_{20}	4.29	3.61	3.77	3.28	3.23	2.70	2.18	0.86	0.51	0.43
C_{21}	4.01	3.43	3.58	3.11	3.07	2.46	2.05	0.86	0.60	0.50
C_{22}	3.53	2.94	3.02	2.66	2.62	2.08	1.74	0.80	0.60	0.53
C_{23}	3.09	2.74	2.83	2.47	2.46	1.90	1.60	0.76	0.63	0.59
C_{24}	2.51	2.31	2.43	1.99	2.09	1.52	1.32	0.66	0.62	0.62
C_{25}	2.46	2.25	2.25	2.07	2.02	1.42	1.24	0.66	0.67	0.70
C_{26}	1.78	1.78	1.72	1.48	1.59	1.06	0.95	0.51	0.60	0.65
C_{27}	1.60	1.58	1.58	1.46	1.39	0.95	0.85	0.54	0.64	0.77
C_{28}	1.30	1.32	1.35	1.34	1.21	0.77	0.69	0.51	0.70	0.80
C_{29}	1.13	1.20	1.03	1.12	0.92	0.59	0.54	0.42	0.76	0.61
C_{30}	1.03	1.23	1.29	1.34	1.09	0.61	0.58	0.61	1.03	0.98
C_{31}	0.51	0.59	0.64	0.68	0.58	0.31	0.28	0.33	0.63	0.67
C_{32}	0.29	0.29	0.29	0.27	0.26	0.14	0.12	0.20	0.37	0.32
C_{33}	0.29	0.34	0.36	0.51	0.35	0.19	0.20	0.34	0.75	0.57
C_{34}	0.06	0.07	0.06	0.07	0.07	0.03	0.03	0.07	0.11	0.11
C_{35}	0.02	0.03	0.03	0.01	0.02	0.01	0.01	0.02	0.01	0.02
Total	61.76	50.25	51.18	45.24	42.39	36.00	28.87	12.27	10.77	10.27

35.13% and 21.50%, respectively. The relative contents of Al_2O_3 and K_2O showed an increasing tendency, whereas CaO was decreased as weathering increased.

4.3.3. Trace elements and REEs

The trace element and REE compositions of the FH-series samples are listed in Tables S3 and S4. A comparison of the concentrations among the sample suite shows that some elements changed substantially during weathering, which can be confirmed by the CV values. Among the large-ion lithophile elements (LILE; Mn, Rb, Ba, Sr, Pb, Cs, Th, and U), Rb, Cs, and K are Group IA elements with similar chemical properties. Rb and Cs may migrate to replace K in mineral form (isomorphism) and become enriched during weathering. As weathering increases, the U content tends to decrease, while the Sr, Th, Rb, and Cs contents tend to increase. Among the transitional elements (TE; Zn, V, Cr, Cu, Ni, Co, and Sc), various oxidation states can be exhibited owing to their high mobility. Therefore, there is a tendency for their elemental content to increase during weathering, except for Sc, which does not change substantially. Among high-field-strength elements (HFSE; Zr, Ga, Nb, Hf, Ta, and Ti), their relatively stable geochemistry (they are insoluble in water) makes them less susceptible to metamorphism, alteration, and weathering. The overall trend is that the loss of soluble fractions increases with weathering owing to leaching. Among the other trace elements (Mo, Li, Sb, Cd, Tl, W, Bi, In, and Be), only Mo content gradually decreased with increased weathering.

The REE contents and associated geochemical parameters of the source rock samples are listed in Table S4. REEs are classified into light REEs (LREEs, La to Pm), middle REEs (MREEs, Sm to Dy), and heavy REEs (HREEs, Ho to Lu) (Tang et al., 2018). ∑REE, ∑LREE, ∑MREE, and ∑HREE are typically used to illustrate REE composition. The normalisation of the North American shales (NASC) shows that the overall REE content of these samples is lower than that of NASC, and the overall curves are smooth and sloping, indicating an enrichment of LREEs and depletion of HREEs (Fig. 7).

5. Discussion

5.1. Determination of the degree of weathering

5.1.1. Major elements indicator

Different chemical weathering indices, such as the chemical index of alteration (CIA), chemical index of weathering (CIW), plagioclase index of alteration (PIA), and A-CN-K diagram index, have been proposed by many scholars to characterise the degree of weathering (Nesbitt and Young, 1982; Harnois, 1988; Tang et al., 2018; Krzeszowska, 2019). CIA (Nesbitt and Young, 1982) and PIA (Fedo et al., 1995) are defined as follows:

$$CIA = \left[\frac{Al_2O_3}{Al_2O_3 + CaO^* + Na_2O + K_2O}\right] \times 100, \quad (1)$$

and

$$PIA = \left[\frac{Al_2O_3 - K_2O}{Al_2O_3 + CaO^* + Na_2O - K_2O}\right] \times 100. \quad (2)$$

The unit of the oxide in the equation is molar, and CaO* is the amount of CaO in the silicate mineral. Because the content of CaO in silicate minerals is comparable to that of Na_2O, when the number of moles of CaO is greater than that of Na_2O, the number of moles of CaO should be equal to that of Na_2O. The CIA was calculated to range from 68.39 to 72.16 with an average value of 69.63 and a CV of 1.54%. PIA is also comparable to CIA, ranging from 67.45 to 82.12 (Table 5). The trend of chemical weathering and changes in major elements and minerals during weathering can be reflected in the A-CN-K ternary diagram. The weathering trend line of these samples is parallel to the A-CN axis, indicating that plagioclase and carbonate minerals were the first to decompose during the weathering of source rocks, contributing to the leaching loss of Ca, Na, and Mg elements. K elements were in a stable state and Al elements were enriched, suggesting that the formation of clay minerals such as montmorillonite and illite was facilitated by increased weathering (Fig. 8A). Furthermore, the data from the weathering profiles were concentrated around the UCC-NASC-PAAS chemical weathering trend line, suggesting that the Yanchang Formation shales in the Yishicun Profile originated mainly from upper continental crust.

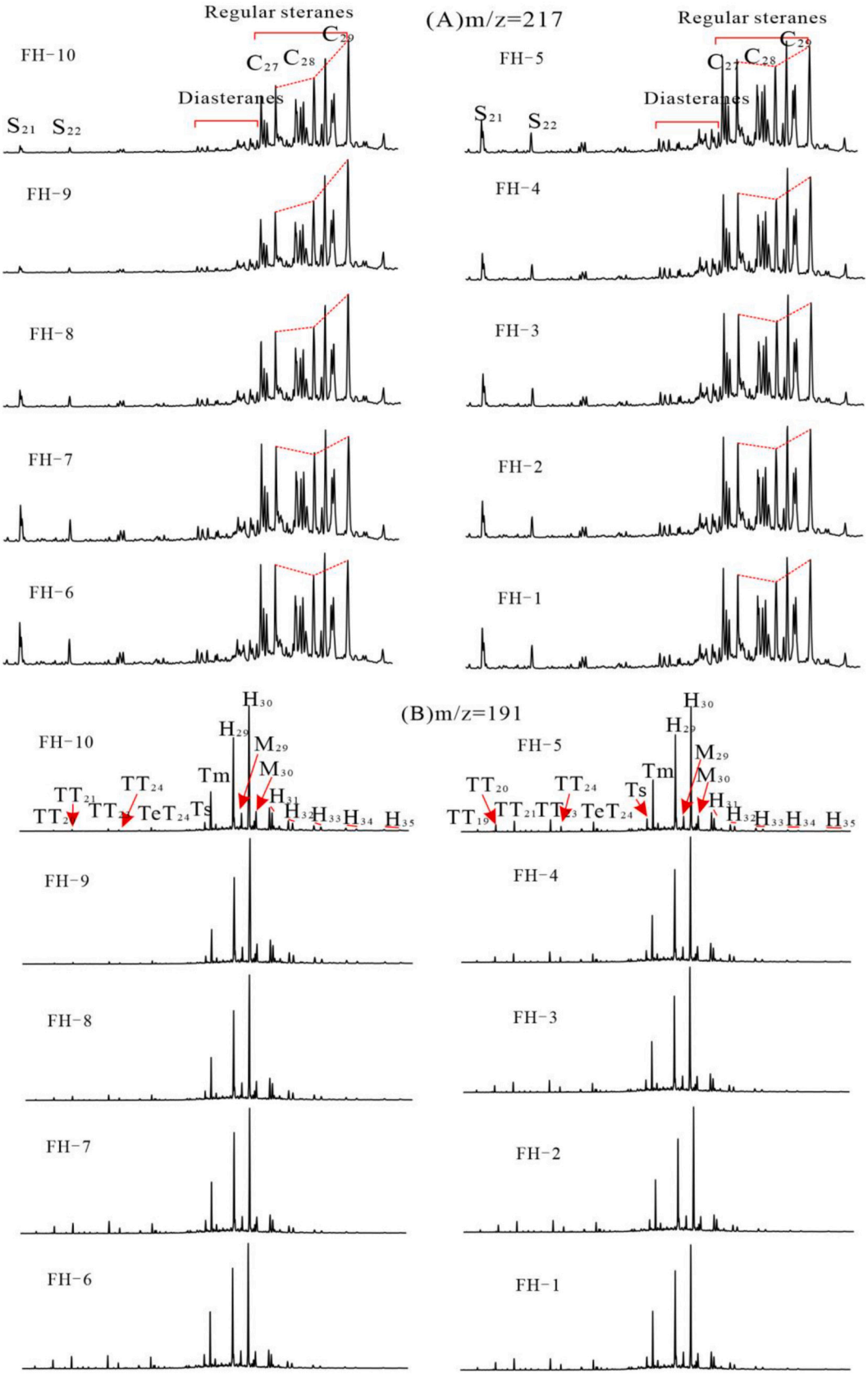

Fig. 5. (A) *m/z* 217 mass chromatograms displaying steranes and (B) m/z 191 mass chromatograms displaying terpanes of saturated hydrocarbon for source rock samples; S_{21}, pregnane; S_{22}, homopregnane; TT_{19-24}, C_{19}–C_{24} tricyclic terpanes; TeT_{24}, C_{24} tetracyclic terpanes; Ts, C_{27} 18α(H)-22,29,30-trisnorhopane; Tm, C_{27} 17α(H)-22,29,30-trisnorhopane; M_{29}, C_{29} 17β(H),21α(H)-30-normoretane; M_{30}, C_{30} 17β(H),21α(H)-moretane; H_{29-35}, C_{29}–C_{35} pentacyclic hopanes.

Table 4
Concentrations of selected PAHs (in μg/g TOC) for source rocks from the Yishicun Profile in the Tongchuan area, Ordos Basin.

	FH-10	FH-9	FH-8	FH-7	FH-6	FH-5	FH-4	FH-3	FH-2	FH-1	Mean	CV (%)
1-MP	0.05	0.04	0.22	0.17	0.30	0.16	0.22	0.18	0.17	0.26	0.18	46.22
2-MP	0.05	0.04	0.24	0.15	0.28	0.16	0.14	0.16	0.15	0.23	0.16	47.72
3-MP	0.02	0.01	0.07	0.05	0.13	0.07	0.03	0.06	0.05	0.06	0.06	62.04
9-MP	0.05	0.03	0.11	0.13	0.30	0.16	0.13	0.17	0.16	0.21	0.14	53.15
DBT	0.002	0.008	0.009	0.008	0.004	0.008	0.014	0.037	0.039	0.027	0.02	86.65
P	0.15	0.11	0.42	0.37	0.85	0.49	0.30	0.33	0.26	0.27	0.35	58.97
TAS_{20}	0.01	0.03	0.09	0.08	0.06	0.03	0.29	0.24	0.30	0.38	0.15	90.48
TAS_{21}	0.01	0.04	0.09	0.09	0.06	0.03	0.29	0.26	0.31	0.39	0.16	88.33
$TAS_{26}20R + {}_{27}20S$	0.21	0.86	1.33	1.19	1.31	1.20	2.42	1.68	2.15	3.50	1.58	57.86
$TAS_{26}20S$	0.05	0.21	0.33	0.29	0.08	0.05	0.76	0.47	0.55	0.89	0.37	79.54
$TAS_{27}20R$	0.12	0.53	0.81	0.70	0.16	0.11	1.45	1.19	1.46	2.12	0.87	78.41
$TAS_{28}20R$	0.15	0.75	1.09	0.98	0.20	0.14	2.29	1.62	1.89	2.96	1.21	80.04
$TAS_{28}20S$	0.22	0.99	1.43	1.31	0.30	0.21	2.84	2.07	2.41	3.71	1.55	77.26
Py	0.04	0.05	0.13	0.09	0.14	0.06	0.13	0.20	0.22	0.27	0.13	57.52
Chr	0.30	0.95	1.48	1.17	0.68	0.30	1.62	0.82	0.91	1.74	1.00	50.69
Fl	0.03	0.08	0.17	0.25	0.13	0.12	0.08	0.14	0.12	0.15	0.13	47.44

MP: methyl phenanthrene, DBT: dibenzothiophene, P: phenanthrene, TAS: triaromatic steroid, Py: pyrene, Chr: chrysene, Fl: fluoranthene.

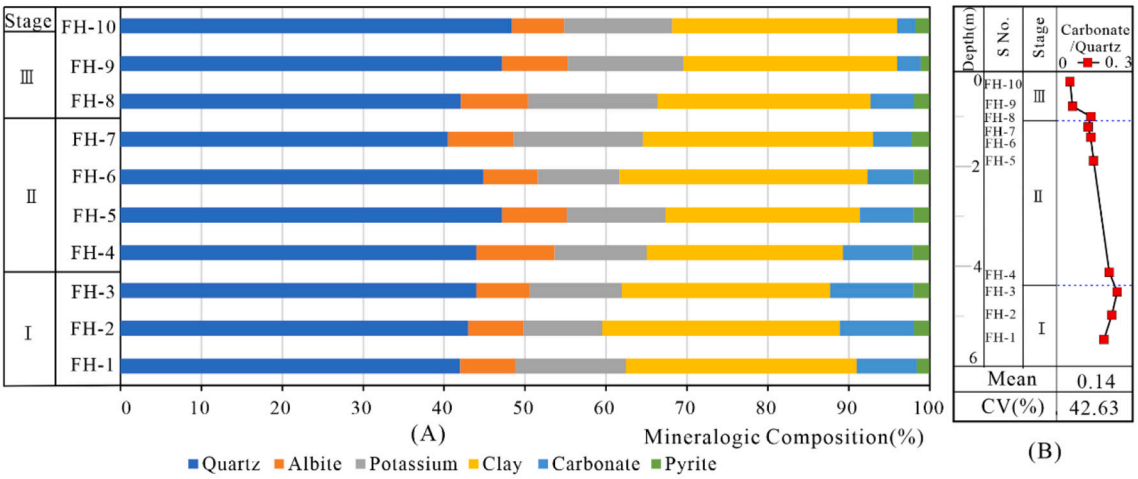

Fig. 6. (A) Stacked bar chat of mineral composition (B) carbonate/Quartz for source rocks from the Yishicun Profile in the Tongchuan area, Ordos Basin.

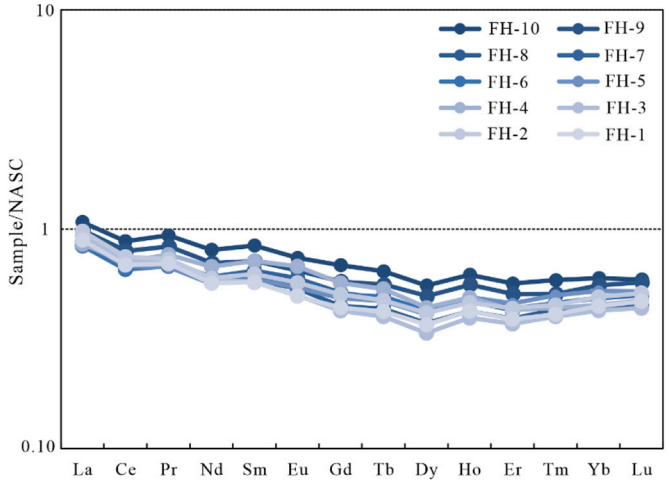

Fig. 7. Spider diagram of REEs for the FH-series samples when normalized to NASC (the North American Shales; Haskin et al., 1968).

According to the cross-plot of CIA versus Na/K (Fig. 8B), all samples were moderately weathered. As the number of samples decreased, the CIA index increased substantially, indicating a pronounced increase in weathering.

5.1.2. Mineral alterations

In the present study, carbonate minerals and pyrite were substantially depleted in the FH-series samples. The reasons for this are as follows: First, the dissolution of carbonate minerals is promoted by sufficient H^+ provided by atmospheric rainfall and pyrite weathering. The decomposition of related minerals in source rocks can also be accelerated by an increase in the permeability and porosity of rocks (Littke et al., 1991; Petsch et al., 2005). Second, the presence of a large area of soil/vegetation cover at the top and bottom of the Yishicun Profile, a warm and humid climate in the Tongchuan area, and the activity of surface water would favour the dissolution and leaching of carbonate minerals. Notably, the pyrite content was relatively low in the overall mineral composition. The main reason for this may be that pyrite (an extremely sensitive mineral) was affected by weathering on the side of the profile, despite the relative freshness of the samples during collection.

Minerals have distinct weathering rates under the same surface conditions. Therefore, the degree of weathering can be estimated by the relative loss or enrichment of the minerals (Littke et al., 1991; Marynowski et al., 2011a; Tang et al., 2018). Littke et al. (1991) suggested that the presence of pyrite may indicate the degree of weathering of source rocks, as pyrite is the mineral most susceptible to weathering (Petsch et al., 1999; Tuttle et al., 2014; Wildman et al., 2004). Tang et al. (2018) estimated that a 40% loss of feldspar, 15% enrichment in clay minerals, and 26% loss of pyrite represented a weak-to-moderate degree of weathering. In this study, the loss of carbonate minerals was

Table 5
Parameters of the palaeosedimentary environment for source rocks from the Yishicun Profile in Tongchuan of the Ordos Basin.

	CIA	PIA	Sr/Ba	U/Th	Ni/Co	V/(V + Ni)	V/Cr	Mo (ug/g)	AU	δU	P/Ti	Sr/Cu
FH-1	69.34	68.84	0.54	4.91	5.05	0.97	8.49	93.6	44.27	1.87	0.46	2.65
FH-2	69.02	68.69	0.48	4.42	5.14	0.97	8.1	101	45.4	1.86	0.44	2.65
FH-3	68.89	67.45	0.44	4.77	4.48	0.97	7.57	101	46.78	1.87	0.42	2.51
FH-4	68.84	68.33	0.44	4.96	4.39	0.95	7.73	69.8	44.68	1.87	0.42	2.87
FH-5	68.39	67.49	0.56	5.28	4.54	0.95	6.45	71.4	51.15	1.88	0.38	3.5
FH-6	69.41	69.95	0.56	4.85	5.27	0.96	7.24	66	46.93	1.87	0.37	1.9
FH-7	70.29	79.94	0.5	4.43	4.85	0.95	7.46	63.4	43.83	1.86	0.32	2.87
FH-8	69.79	78.52	0.6	3.79	5.49	0.95	6.96	69	35.3	1.84	0.32	3.64
FH-9	70.2	78.72	0.75	3.16	5.31	0.94	6.91	74.3	32.47	1.81	0.39	3.34
FH-10	72.16	82.12	0.86	2.9	5.34	0.93	6.8	77.8	32.22	1.79	0.39	4.19
Mean	69.63	73.01	0.57	4.35	4.99	0.95	7.37	78.73	42.30	1.85	0.39	3.01
CV%	1.54	8.20	23.36	18.48	7.96	1.59	8.49	18.25	15.54	1.61	11.74	21.86

AU, U − Th/3; δU, 2 U (U + Th/3).

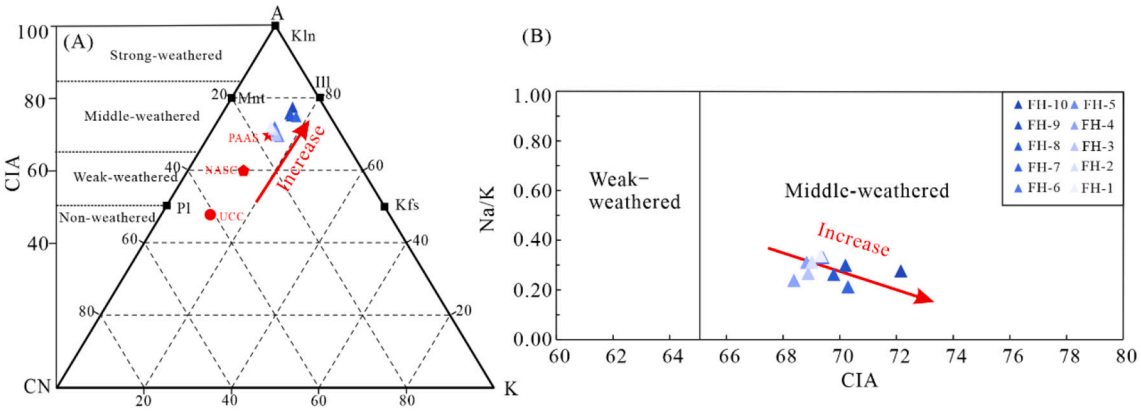

Fig. 8. (A) A-CN-K ternary diagram, A: Al2O3; CN: CaO* + Na2O; K: K2O; UCC: Upper Continental Crust; NASC: North American shales; PAAS: the post-Archean Australian Shale; Kln: Kaolinite; Mnt: Montmorillonite; Ill: Illite; Pl: Plagioclase; Kfs: K-feldspar; (B) cross plots of CIA index against Na/K ratio showing the weathering degree for the FH-series samples (Wu et al., 2016).

approximately 77%, with a very low pyrite content of approximately 2% (Table S1, Fig. 6), which is consistent with the moderate degree of weathering indicated by the CIA.

5.1.3. Organic matter variation

OM may be susceptible to varying degrees of oxidation, water leaching, and biodegradation during weathering, which not only results in a decrease in the OM content but also in molecular composition of the EOM. Clayton and King (1987) showed that sterane distribution was substantially altered during weathering, whereas pentacyclic triterpenes were not affected. Marynowski et al. (2011a) reported that the distributions of steranes and hopanes were affected by weathering, and steranes were less resistant to weathering than hopanes. Although the extent of weathering varies, certain characteristic effects are recognisable (Clayton and Swetland, 1978). This indicates that the depletion of specific compound groups depends on their molecular stability during weathering. In other words, the change in certain compound groups during weathering may be related to the degree of weathering. Therefore, it is essential to assess the degree of weathering of the source rocks based on OM changes, mineral alteration, and elemental characteristics. The specified variations in OM in this study are discussed in detail below.

By comparing the organic and inorganic geochemical characteristics of the source rock samples across the outcrop profile (Figs. 2, 3, 6B, 14, and 15), it is notable that many parameters show an opposite tendency for those samples in Stage I compared to the samples in Stage III. These include TOC, EOM, Rock-Eval parameters (TOC, S1, S2, and HI), Sat/Aro, Carbonate/Quartz, Mo content, and DBT/P. The data indicate that the samples in Stage III were severely altered, and the weathering of the samples occurred mainly at depths up to 2 m below the surface soil/vegetation cover. Moreover, this provides geochemical evidence to demonstrate that the samples in Stage I were weathered mainly in the opposite direction owing to the influence of the soil and vegetation cover at the bottom of the profile (Fig. 1C, green line). Based on these results, the pathway and degree of weathering were determined (Fig. 1C).

5.2. Element fractionation and the impact on elemental analysis applications

5.2.1. Major elements

The characteristics of major elements during weathering depends on the form in which they are present in the shale and their activities. For instance, Si, which is present in quartz and is more resistant to weathering, is more abundant in the sample suite. Ca is mainly present in shale in the form of carbonate minerals, which are highly mobile and soluble under acidic conditions. The CaO content correlates well with the carbonate mineral content ($R^2 = 0.73$), and both decreased substantially with increased weathering (Fig. 9), which suggests that the depletion of Ca is mainly related to the loss of carbonate minerals from source rocks by weathering decomposition and leaching.

5.2.2. Trace elements and related palaeoenvironmental parameters

5.2.2.1. Redox conditions. Trace elements are sensitive to environmental variation. Therefore, redox-sensitive element parameters [e.g. V/Cr, V/(V + Ni), U/Th, Ni/Co, and δU] in fine-grained sediments have been widely used for palaeosedimentary environmental discrimination (Wignall, 1994; Wedepohl, 1995; Sageman and Lyons, 2003; Qiao et al.,

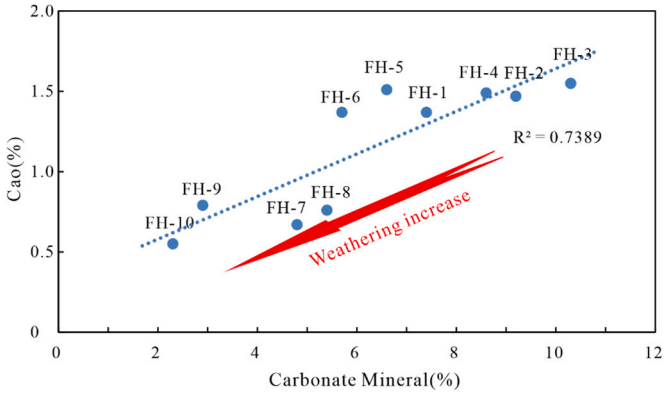

Fig. 9. Correlation diagram between Cao and carbonate minerals for the FH-series samples.

2022). Ni is commonly used as a redox-sensitive element (Brumsack, 2006). Under reducing conditions, Ni can be bound to pyrite (NiS) or tetrapyrrole complexes (geoporphyrins), which accumulate in sediments (Baker and Louda, 1986). Jones and Manning (1994) suggested that anoxic marine conditions favour the concentration of V in OM by binding V^{4+} to porphyrins, whereas Cr is usually concentrated in the detrital sediment fraction (Tuttle et al., 2009). The V/(V + Ni) ratio, as defined by Hatch and Leventhal (1992), Ni/Co, as defined by Jones and Manning (1994), and V/Cr can reflect the stratification and redox conditions of sedimentary waters. According to Tables S3 and 5, the V/(V + Ni), V/Cr, and Ni/Co ratios are in the range of 0.93–0.97 (CV = 1.59%), 6.45–8.49 (CV = 8.49%), and 4.39–5.49 (CV = 7.96%), respectively. Each of these parameters indicate that the sedimentary water conditions the source rocks were anaerobic. Although the variation in these parameters was small (CV < 10%), there was a slight decrease in the V/(V + Ni) and V/Cr ratios, and a slight increase in the Ni/Co ratio during weathering (Fig. 10).

Uranium is highly sensitive to variations in redox conditions (Wignall, 1994). U^{4+} in uranium-containing minerals is oxidised to more soluble U^{6+} in an oxic environment, leading to U dissolution migration (Panahi et al., 2000), which results in the depletion of U under weathering. Tuttle et al. (2009) and Marynowski et al. (2017) investigated trace element variations in related profile during weathering and suggested that the decrease in U concentration was largely associated with OM. However, Th is immobile, insoluble in surface water, and present in residual minerals during weathering (Jones and Manning, 1994). As shown in Table 5 and Fig. 10, the CV values of U/Th (mean = 4.35), δU (mean = 1.85), and AU (mean = 42.30) are 18.48%, 1.61%, and 15.54%, respectively, which are typically interpreted to reflect the anaerobic water column (Cao et al., 2012; Li et al., 2017).

Molybdenum is also strongly influenced by redox conditions (Brumsack, 2006; Qiao et al., 2022). Mo dissolves in water in the high-valent state (Mo^{6+}) under oxidising conditions. Under reducing conditions, Mo is enriched in sediments in the low-valent state of Mo^{4+}. Wildman et al. (2004) and Marynowski et al. (2017) discovered that Mo is mainly hosted in pyrite and MoS in shale and that the rapid weathering of pyrite may lead to removal of Mo from shale. Our results demonstrated Mo ranges from 63.4 μg/g to 101 μg/g with a mean value of 78.73 μg/g and a CV of 18.25%. This indicates an anaerobic reducing environment (Algeo and Tribovillard, 2009) and a very rapid depletion of Mo across the weathering profile (Table 5 and Fig. 10).

5.2.2.2. Palaeosalinity. Several studies have shown that the Sr/Ba values in shales can be used to reconstruct palaeosalinity (Pan et al., 2021). This study found an apparent enrichment of Sr (CV = 22.82%) and obscure change of Ba (CV = 10.26%) in these samples (Table S3). The Sr/Ba ratios range from 0.44 to 0.86, with a CV of 23.36% (Table 5 and Fig. 10). Sr/Ba gradually increases with weathering, and its palaeosalinity interpretation could change from a freshwater to brackish water environment.

5.2.2.3. Palaeoclimate. In continental basins, a high concentration of Sr is generally related to the strong evaporation of lake water in arid and hot climates. The Sr/Cu ratio can also be applied in judging palaeoclimate (Pan et al., 2021). The Sr/Cu ranges from 1.9 to 4.19 with a CV of 21.86% (Table 5 and Fig. 10), indicate that the climate was mainly warm and humid during the deposition of source rocks in the Yishicun Profile. The Sr/Cu ratio tends to gradually increase with increasing weathering, and its palaeoclimatic interpretation is closer to a dry and hot environment.

5.2.2.4. Palaeoproductivity. The P/Ti ratio is commonly used to characterise the trophic status of palaeolakes (Algeo et al., 2011; Pan et al., 2021). According to Table 5 and Fig. 10, the P/Ti values of the samples range from 0.32 to 0.46 with a CV of 11.74%, ranging between moderate productivity (Ubara section, average chert P/Ti ratio of 0.34) and high productivity (Ubara section, average black shale P/Ti ratio of 0.79), which indicates moderate palaeoproductivity during their deposition. It should be noted that there was a decreasing tendency for P/Ti with increasing weathering, which would lead to a lower productivity bias in the palaeoproductivity interpretation of this indicator.

5.2.2.5. Provenance. The Sc-La-Th ternary diagram is commonly used

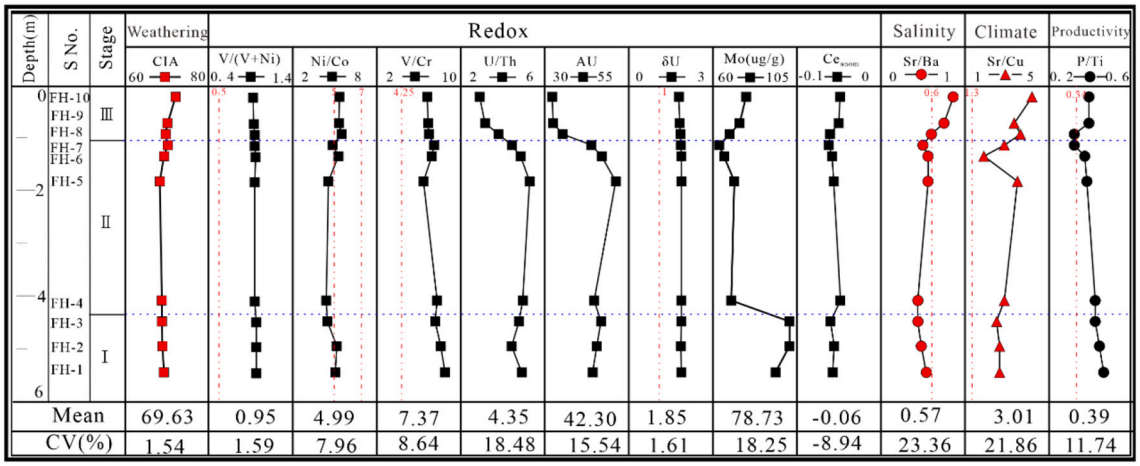

	CIA	V/(V+Ni)	Ni/Co	V/Cr	U/Th	AU	δU	Mo(ug/g)	Ce	Sr/Ba	Sr/Cu	P/Ti
Mean	69.63	0.95	4.99	7.37	4.35	42.30	1.85	78.73	-0.06	0.57	3.01	0.39
CV(%)	1.54	1.59	7.96	8.64	18.48	15.54	1.61	18.25	-8.94	23.36	21.86	11.74

Fig. 10. Composite depth plot of sedimentary environment parameters for source rocks from the Yishicun Profile in Tongchuan of Ordos Basin.

to explore mineral origin (Bhatia and Crook, 1986; Diskin et al., 2011). Sc-La-Th elements were concentrated throughout the weathered series of samples, which is comparable to the distribution of UCC (Fig. 11), indicating that the REE composition and their relative ratios remain applicable to the determination of their origin. This provenance explanation is consistent with the discussion above for the A-CN-K ternary diagram.

5.2.3. REEs

REEs are generally conserved during weathering and transportation to the ocean with fine-grained suspended sediment. However, the weathering of shales and the consequent dissolution of phosphate minerals cause the depletion of REEs, especially MREEs (McArthur and Walsh, 1984; Hannigan and Sholkovitz, 2001; Ma et al., 2011). Ce_{anom}, proposed by Wright et al. (1987) to describe the degree of Ce anomalies, is usually applied to discriminate redox environments. According to Table S4 and Fig. 10, the Ce_{anom} values of all the samples were greater than −0.1, indicating reducing dysoxic water volume environments. It is notable that the REEs content in these samples appears to have increased slightly during weathering, which is inconsistent with previous reports (Hannigan and Sholkovitz, 2001; Marynowski et al., 2017; Tang et al., 2018). This phenomenon is mainly caused by the horizontality of the sampled profile (Fig. 1C), which results in the re-deposition of REEs in the soil cover at depth owing to dissolution and untimely leaching during shale weathering. Jin et al. (2017) also observed this phenomenon and explained that REEs can be dissolved near the surface and re-deposited at depth due to changes in DOC, pH, and clay surface area during weathering. The CV of ∑LREE, ∑MREE, and ∑HREE are 11.17%, 16.49%, and 12.83%, respectively. As weathering increased, ∑REE values gradually increased, and ∑LREE, ∑MREE, and ∑HREE also showed increasing trends. However, the CV of ∑MREE is greater than those of ∑LREE and ∑HREE, indicating that MREE has a more significant variation than LREE and HREE, and the MREEs are preferentially affected during weathering.

5.3. Impact on source rock evaluation

Petroleum resource assessment of source rocks is one of the fundamental stages of petroleum exploration and development, providing reliable geochemical information to focus exploration activities on a certain place and optimise risks (Ramos, 2015; Abd-Allah et al., 2019). However, in the early stages of exploration and development, owing to limited drilling and coring, outcrop samples are commonly used to characterise source rocks and conduct organic geochemical investigations (Clayton and Swetland, 1978). Weathering has a substantial influence on the organic geochemical characteristics of source rocks, resulting in a remarkable depletion in the amount of their OM and alterations in their chemical composition and structure (Leythaeuser, 1973; Clayton and Swetland, 1978; Petsch et al., 2000, 2001; Marynowski et al., 2011b; Tamamura et al., 2015).

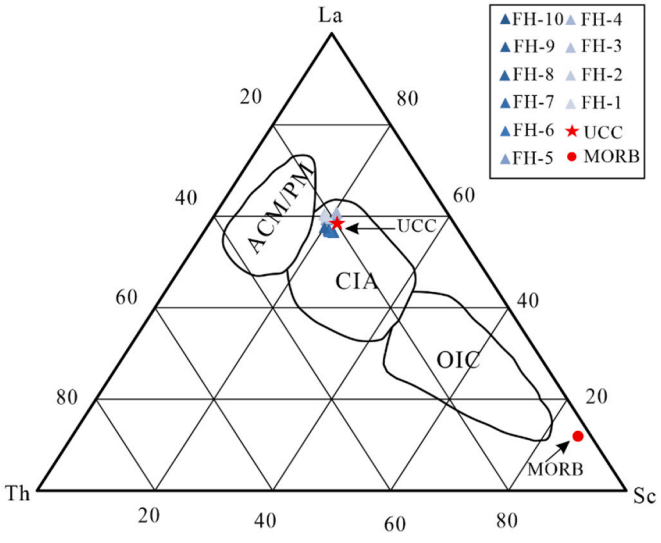

Fig. 11. Sc-La-Th ternary diagram illustrating the relationship of FH-series samples and the UCC as well as the Indian Ocean MORBs (Duliu et al., 2009); UCC, upper continental crust (Taylor and McLennan, 1985); PM, passive continental margin; ACM, active continental margin; CIA, continental island arc; OIA, oceanic island arc.

5.3.1. Abundance of OM

These results show a gradual decrease in TOC, S1 + S2, and EOM with increased weathering (Table 1; Fig. 2). Specifically, TOC decreased from 24.46% (an average in Stage I, similarly hereinafter) to 14.44% (FH-10, similarly hereinafter); S1 + S2 decreased from 81.86 mg/g to 30.01 mg/g; EOM decreased from 12.34 mg/g to 3.12 mg/g, with losses of 40.96%, 63.34%, and 74.71%, respectively. This is higher than the shale weathering of the Upper Cretaceous Mancos Shale (approximately 25% TOC loss and 50% soluble OM loss; Leythaeuser, 1973), and much lower than the Carboniferous marine shale in the Holy Cross Mountains (97% TOC loss and 75% soluble OM loss; Marynowski et al., 2011a), and similar to the weathering studied by Meng et al. (1999) for outcrops of source rocks in the Xining Basin (58.96% TOC loss and 77.59% soluble OM loss). It is notable that the loss of EOM is consistently higher than the loss of TOC, irrespective of the degree of weathering which had affected the source rocks, reflecting the fact that weathering is more destructive to soluble OM than solid OM.

Not only is the amount of OM affected by weathering (Table 1, Fig. 2), the compositional characteristics of EOM can also be affected (Table 1; Fig. 3). The relative content of the EOM bulk composition changed during weathering, and the content of saturated and aromatic hydrocarbons decreased with a loss of 51.89% and 79.18%, respectively. The resin and asphaltene content increased by 15.91% and 63.39%, respectively. The relative contents of the resin and asphaltene fractions are much higher than those of saturated and aromatic hydrocarbons, which can be attributed to low maturity of OM in these samples. In addition, saturated hydrocarbons are relatively less depleted than aromatic hydrocarbons, resulting in a high saturated/aromatic ratio in samples in Stage III compared to the samples in Stage I (Table 1, Fig. 3). Specific components of soluble OM have distinct capacities to resist weathering. Clayton and Swetland (1978) also reported that the aromatic fraction is preferentially depleted relative to the saturated fraction during weathering. It has been reported that the water solubility of aromatic compounds is approximately 200 times that of normal alkanes with the same CNs (Price, 1976; McAuliffe, 1979; Lafargue and Barker, 1988; Fig. 12), which would cause aromatic hydrocarbons to be washed by surface water during weathering (Palmer, 1993; Skręt et al., 2010).

5.3.2. Type and source of OM

Determination of the OM type and source is important for evaluating the hydrocarbon potential of source rocks. In the cross plot of HI versus T_{max} (Fig. 13A), the OM types of these samples were mainly types II_1 and II_2. During oxidative weathering, T_{max} does not change substantially, the HI gradually decreases, and the OI gradually increases due to the incorporation of oxygen into the OM (Table 1), which results in a downward distribution of data points and a worse interpretation of OM types. A similar change was observed in the elemental composition of the kerogen. An increase in the kerogen O/C ratios and a slight decrease in the H/C ratios were observed in these samples. The kerogen N/C ratios remained low and constant (Table 1, Fig. 13D). This finding is consistent with the results of Petsch et al. (2000, 2005). Concurrently, a substantial decrease in the alkyl-CH_2- and -CH_3 groups and a pronounced increase in the C = O bond were revealed by Petsch et al. (2000) based on an infrared analysis of kerogen. This suggests that oxygen can also be incorporated into kerogen molecular structure during

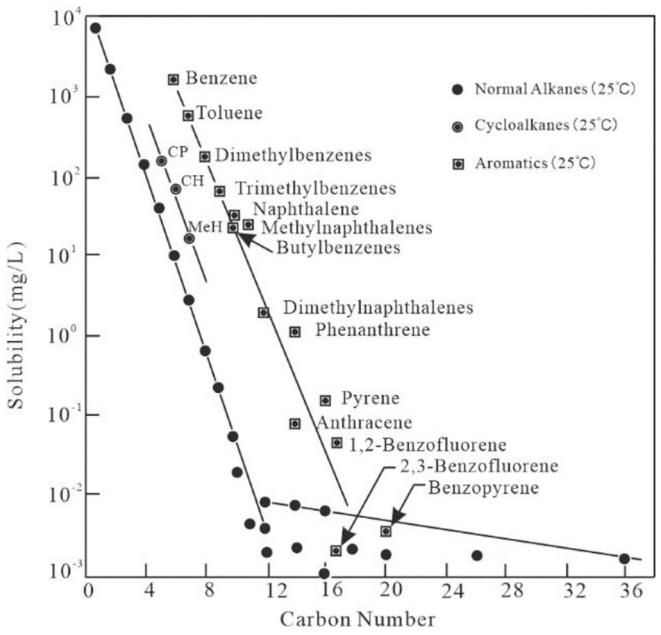

Fig. 12. Solubilities of normal *n*-alkanes, aromatic hydrocarbons, and naphthenes (cycloalkanes) in water as a function of CN (from McAuliffe, 1979, with additions from Price, 1976); CP, cyclopentane; CH, cyclohexane; McH, methylcyclohexane.

weathering, leading to a partial distortion of the OM type.

The distributions of *n*-alkanes and isoprenoids can be used for OM source analysis (Scalan and Smith, 1970; Peters et al., 2005; Qin et al., 2018). Based on the results for *n*-alkanes and isoprenoids, the low CN *n*-alkanes were severely depleted compared to the high CN *n*-alkanes, which caused setback of the main peak, an increase in TAR, and a sharp reduction in SCh/LCh and $\Sigma C_{21-}/\Sigma C_{22+}$ (Table 2, Fig. 14). This is consistent with previous reports (Clayton and King, 1987; Bjorøy and Vigran, 1980; Marynowski et al., 2011a), but inconsistent with the laboratory results of low-temperature oxidation (Faure et al., 1999). The sedimentary environment and OM type are reflected by Pr/Ph, Pr/nC_{17} and Ph/nC_{18}. Isoprenoid-related parameters remain stable during weathering (Fig. 14), which is consistent with the results of the Marynowski et al. (2011a) shale weathering research. As shown in Fig. 13B, although weathering can slightly alter the distribution of the sample points, the OM type interpretation still remains valid.

The distribution of steranes and terpenes can also be used to reflect the OM source (Peters et al., 2005; Cao et al., 2018). The relative distribution of regular steranes C_{27-29} was gradually transitioned from the typical 'V' type to the inverse 'L' type as weathering increased (Table 2, Figs. 5 and 14). The sample points gradually approached the C_{29} side in the ternary plot (Fig. 13C), and the CV values of the C_{27}-C_{29} regular steranes were 13.11%, 3.22%, and 7.72%, respectively. This is consistent with the observations of Wei et al. (2012), and inconsistent with the findings of Marynowski et al. (2011a), mainly because of the different degrees of weathering suffered by the samples. The distribution of tricyclic terpenes was dominated by TT_{23} in the order $TT_{23} > TT_{21} > TT_{20}$. Their relative content changed like that of steranes during weathering, with an increase in high CN TT_{23} and a significant decrease in low CN TT_{20-21} in Stage III. (Figs. 5 and 15). Furthermore, TT/H_{30} decreased with increased weathering. Marynowski and Wyszomirski (2008) and Clayton and King (1987) reported that oxidation can lead to a change in the relative content of tricyclic terpenes.

In general, as judged from the results of samples in Stage I, where weathering was the weakest, the OM type of the Chang 7 source rocks in the Yishicun Profile is mainly type II, and the sources of OM were phytoplankton and terrestrial plants. This is consistent with the results of Li et al. (2017), who studied the OM source of shales from the Yanchang Formation in the Tongchuan area. In contrast, the data from the most weathered samples in Stage III suggested that weathering has influenced the identification of OM types in the source rocks. The interpretation based on *n*-alkanes may be distorted, while the results based on elemental analysis of kerogen, Rock-Eval data, and some biomarkers (isoprenoids, regular steranes, and tricyclic terpenes) may be slightly influenced but still valid.

5.3.3. Maturity of OM

The vitrinite reflectance (Ro), T_{max} and biomarker parameters are commonly used to assess the maturity of source rocks (Seifert and Moldowan, 1986; Peters et al., 2005; Pan et al., 2021; Zhang et al., 2022). The average value of T_{max} was 432 °C with a CV of 0.35% (Table 1), indicating little change in T_{max} and a low maturity stage of thermal evolution. This implies that weathering has no effect on T_{max} in Rock-Eval. The ααα20S/(20S + 20R) and αββ/(ααα + αββ) for C_{27} and C_{29} steranes, Ts/(Ts + Tm), and 22S/(22S + 22R) for C_{31} and C_{32} homohopanes, are also stable for the samples across the outcrop profile with extremely low CV values (< 8%, Table 2). This is comparable to that reported by Clayton and King (1987). Biomarker parameters of aromatic hydrocarbons, such as the methylphenanthrene index (MPI1, MPIR), can also be used to indicate maturity (Radke, 1988). According to Table 2, the average values of MPI1 and MPIR are 0.45 and 0.65, respectively, indicating a low-maturity thermal evolutionary stage. Although the content of 1-, 2-, 3-, and 9-MP, and P decreased during weathering (Table 4), the variation in their parameters was insignificant (Fig. 14). This is consistent with the variation in MPI in weathering reported by Clayton and King (1987) and inconsistent with the results of Marynowski et al. (2011a). The main reason for this is that the FH-series samples were subjected to weaker weathering than the latter samples. The S_{21-22} pregnanes/C_{27-29} steranes and TAS(C_{20-21})/(C_{26-28}) ratios can also be used to evaluate maturity of crude oils based on the difference in their thermal stability (Mackenzie and McKenzie, 1983; Liu et al., 2022). The average and CV values for S_{21-22}/C_{27-29} and TAS (C_{20-21})/(C_{26-28}) were 0.11, 43.36%, 0.09, and 41.01% (Table 2), respectively, indicating a high degree of data dispersion. A tendency to decrease with increased weathering was shown for these parameters, and this tendency was especially pronounced for those samples in Stage III, which causes the maturity interpretation based on both parameters to be distorted and suggest a lower maturity.

5.4. Analysis of weathering

It is worth noting that low molecular weight biomarkers, such as the low CN *n*-alkanes, S_{21-22} pregnanes, TAS(C_{20-21}) and TT_{20-23}, are more susceptible to depletion by natural weathering than their higher molecular weight counterparts in this study. OM is exposed to the surface for long periods of time, and the preferential loss of the lighter components of EOM may be caused by natural evaporation, diffusion, and water leaching. In fact, in addition to the above factors, photooxidation induced by sufficient light conditions may also lead to a decrease in saturated and aromatic hydrocarbon content and an increase in asphaltene content in EOM (Glattke et al., 2020), which has been demonstrated in offshore oil spills. However, evaporation causes a significant loss in the light hydrocarbon fraction (mostly in the C_7 range) of crude oil or extracts, with only a little impact on the middle to high molecular weight alkanes (C_{12}-C_{35+}) (Cañipa-Morales et al., 2003). Moreover, the evaporation losses of C_5-C_8 *n*-alkanes become more difficult with increasing CNs. The TOC content favours the preservation of light hydrocarbons in shale, even if the high TOC (>11%) shale is exposed in powder form for a long time, the volatility loss of light hydrocarbons is even less. (Jiang et al., 2016). In addition, biodegradation can also alter the *n*-alkanes composition with microorganisms preferentially and selectively consuming the lighter hydrocarbons in the early stages (Peters et al., 2005). In contrast, the short chains of *n*-alkanes

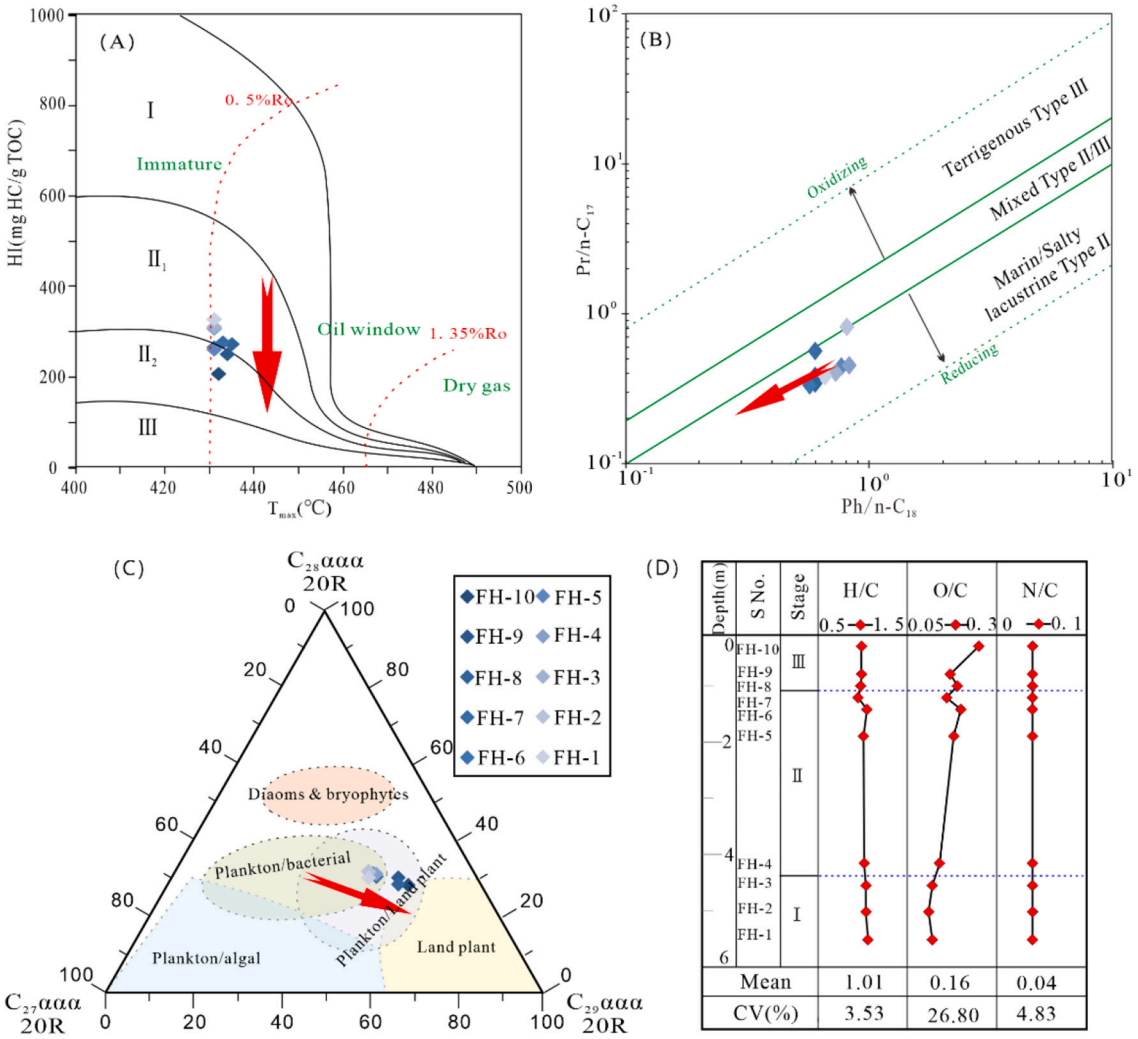

Fig. 13. (A) Cross plots of Rock-Eval HI versus T_{max}; (B) plot of Pr/n-C_{17} versus Ph/n-C_{18} ratios; (C) ternary plot of regular steranes C_{27}–C_{29}; (D) composite depth plot of kerogen elemental composition for source rocks from the Yishicun Profile in Tongchuan of Ordos Basin.

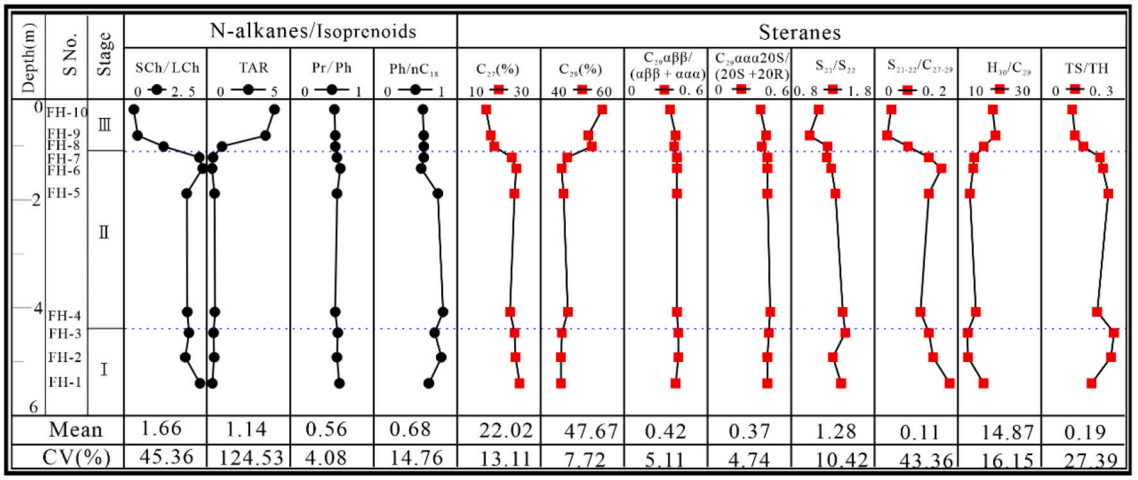

Fig. 14. Biomarker parameters from *n*-alkanes, isoprenoids, and steranes and their related statistical parameters for source rock samples in the Yishicun Profile.

increase while the long chains degrade during low temperature oxidation (Faure et al., 1999). Pan et al. (2017) and Liu et al. (2018) observed that Pr and Ph partly degraded at a moderate biodegradation stage. Moreover, no pronounced biodegradation variations are observed for steranes and hopanes in all weathered samples. Therefore, it is likely that these samples were subjected to a low level of biodegradation. Short

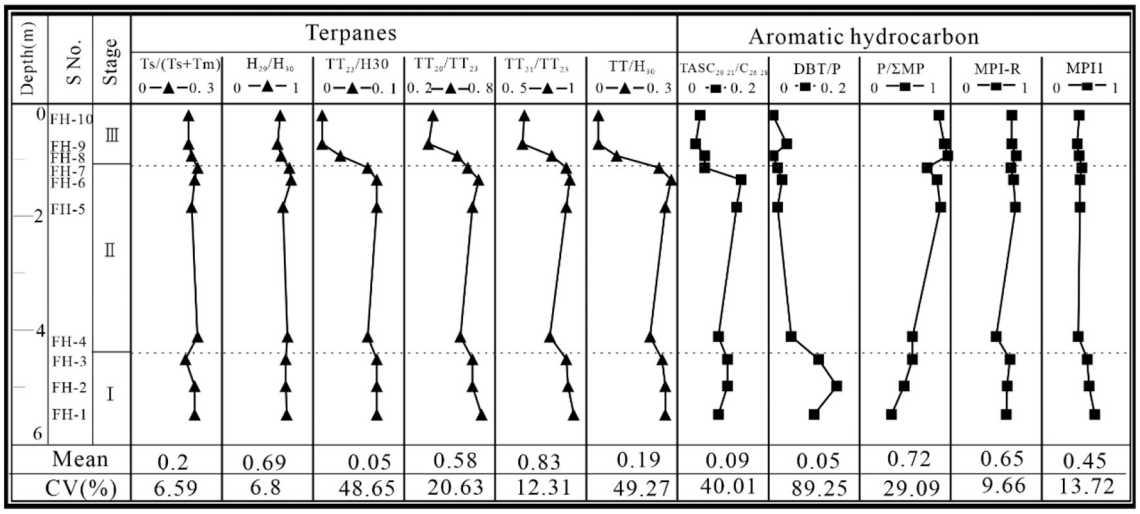

Fig. 15. Biomarker parameters from terpanes and aromatic hydrocarbons and their related statistical parameters for source rock samples in the Yishicun Profile.

sidechain TAS($C_{20–21}$) and $C_{27–29}$ regular steranes were preferentially removed compared to $S_{21–22}$ pregnanes and TAS($C_{26–28}$) during moderate–severe stages of biodegradation (Wardroper et al., 1984; Brooks et al., 1988; Liu et al., 2022). Therefore, the preferential loss of pregnanes in this study was evidently not attributed to biodegradation. TT_{20}, TT_{21} and TT_{23} with extremely high resistance to biodegradation (Peters et al., 2005; Liu et al., 2022), showed a significant change in distribution throughout the weathered sample suite. Therefore, biodegradation, photooxidation, evapotranspiration and low-temperature oxidation are obviously not effective enough to explain the regular changes of these biomarkers during weathering. We think surface water leaching may be another important factor that influence the distribution of biomarkers.

Surface water leaching can change the composition of EOM in a similar way, preferentially removal of low CN alkanes with high water solubility (Palmer, 1993; Skręt et al., 2010). The water solubility of *n*-alkanes decreases exponentially with the increase in their molecular weight (Fig. 12, Eastcott et al., 1988). Low molecular weight PAHs are also preferentially depleted relative to their more stable polycyclic counterparts during weathering. In some detailed studies of EOM, low molecular-weight aromatic compounds, such as naphthalene, dibenzofuran, and dibenzothiophene, are substantially depleted (Gieskes et al., 1990; Marynowski et al., 2011a). Han et al. (2022) studied the hygroscopicity of organic compounds and observed that organic compounds with more water-soluble functional groups, lower molecular weights, and higher O:C ratios tended to exhibit higher hygroscopicity, although this correlation was not linear. As discussed above for the water solubility of biomarkers, the short side chains of pregnane and triaromatic steroids have higher water solubilities than their long side-chain counterparts. This profile was in a mountainous area with steep terrain, and the precipitation in this study area was sufficient with an average annual of ~700 mm, which provides favourable conditions for enough surface water runoff. Meanwhile, it is notable that DBT/P, an indicator of water washing (Palmer, 1984), decreased gradually with increased weathering, except for samples in Stage I. Therefore, besides DBT/P, the preferentialremoval of low molecular weight biomarkers, such as the low CN *n*-alkanes, high-bioresistance $S_{21–22}$ pregnanes, TAS($C_{20–21}$) and $TT_{20–23}$, may be mainly caused by the leaching of surface water during weathering. This suggests that surface water leaching played a substantial role in the weathering of source rocks in the Yishicun Profile.

6. Conclusions

The aim of this study was to examine how natural weathering can produce pronounced changes in bulk, molecular, mineral, and elemental compositions of petroleum source rocks. Detailed investigations of organic and inorganic characteristics have been conducted on a series of weathered source rock samples from the Yishicun Profile in the Tongchuan area of the Ordos Basin to examine the impact of natural weathering on source rocks. The results show that weathering causes systematic changes in the amount and composition of inorganic features (minerals, major and trace elements, and REEs) and OM (kerogen and EOM), and the extent of weathering-induced change is closely related to the degree of weathering. Owing to leaching by surface water and biodegradation, the weathering of samples along the horizontal strata chiefly occurred at a depth of approximately 2 m from the surface soil cover and the bottom of the profile, which could have resulted in a 41% decrease in TOC and a 75% loss of EOM. Furthermore, weathering can cause the loss of saturated and aromatic hydrocarbon fractions. With the increase of resin and asphaltene fractions, aromatic hydrocarbons are relatively more severely depleted than saturated hydrocarbons because of the differences in water solubility. In saturated and aromatic hydrocarbons, low-molecular-weight biomarkers, such as the low CN *n*-alkanes, $S_{21–22}$ pregnanes, $TT_{20–23}$, and TAS($C_{20–21}$), are more susceptible to depletion by natural weathering than their higher molecular weight counterparts due to leaching by surface water. These biomarkers exhibit a similar phenomenon in that those with lower molecular weight are more easily depleted than those with higher molecular weight. For example, S_{21} vs. S_{22} pregnane, C_{27} vs. C_{29} steranes, TT_{20} vs. TT_{23}, and TAS_{20} vs. TAS_{21}. These weathering-induced changes in organic geochemical characteristics also influence the evaluation of hydrocarbon resources based on OM abundance, type, and maturity.

The major element composition shows that the outcrop profile is in a moderate weathering stage, with slight enrichment of HREEs and preferential removal of MREEs. The values of commonly used palaeoenvironmental geochemical proxies, including U/Th, AU, Mo, Sr/Ba, Sr/Cu, and P/Ti, displayed varying degrees of weathering-related alteration (CV > 10%). Other palaeoenvironmental proxies, such as V/(V + Ni), Ni/Co, V/Cr, δU, and Ce_{anom} demonstrated only slight change and remained reliable for environmental interpretation. Therefore, data from organic and inorganic geochemical studies based on outcrop samples should be interpreted carefully.

Author contributions

Conceptualization, Yuhong Liao and Shubiao Pan; methodology, Yuhong Liao and Shubiao Pan; software, Shubiao Pan; validation, Yuhong Liao and Bin Jiang; formal analysis, Shubiao Pan; investigation, Yuhong Liao, Shubiao Pan, Zhixiong Wan and Fu Wang; resources,

Yuhong Liao and Bin Jiang; data curation, Shubiao Pan and Zhixiong Wan; writing—original draft preparation, Shubiao Pan; writing—review and editing, Yuhong Liao and Shubiao Pan; visualization, Yuhong Liao and Shubiao Pan; supervision, Yuhong Liao; project administration, Yuhong Liao; funding acquisition, Yuhong Liao. All authors have read and agreed to the published version of the manuscript.

Declaration of Competing Interest

The authors declare that they have no known competing financial interests or personal relationships that could have appeared to influence the work reported in this paper.

Acknowledgements

The financial support for this study was funded by the National Natural Science Foundation of China (Grant No. 41872156 and 42173056). This is contribution No.IS-3255 from GIGCAS. The authors thank two anonymous reviewers for their valuable comments that helped to greatly improve the content and quality of the paper. We are also indebted to Shifeng Dai, editor-in-chief, for his great help and patience in handling the manuscript.

Appendix A. Supplementary data

Supplementary data to this article can be found online at https://doi.org/10.1016/j.coal.2022.104119.

References

Abd-Allah, Z.M., Abdullah, W.H., Abdel-Fattah, M.I., 2019. Assessment of Eocene, Paleocene and cretaceous source rocks in the West Feiran area, offshore Gulf of Suez. Egypt. J. Pet. Sci. Eng. 180, 756–772. https://doi.org/10.1016/j.petrol.2019.05.073.

Algeo, T.J., Tribovillard, N., 2009. Environmental analysis of paleoceanographic systems based on molybdenum–uranium covariation. Chem. Geol. 268, 211–225. https://doi.org/10.1016/j.chemgeo.2009.09.001.

Algeo, T.J., Kuwahara, K., Sano, H., Bates, S., Lyons, T., Elswick, E., Maynard, J.B., 2011. Spatial variation in sediment fluxes, redox conditions, and productivity in the Permian–Triassic Panthalassic Ocean. Palaeogeogr. Palaeoclimatol. Palaeoecol. 308, 65–83. https://doi.org/10.1016/j.palaeo.2010.07.007.

Alkhafaji, M.W., 2021. Biomarker assessment of oil biodegradation, water washing, and source rock characteristics of oil seeps from the Foothill Zone along the Tigris River Northern Iraq. J. Pet. Sci. Eng. 197, 107946 https://doi.org/10.1016/j.petrol.2020.107946.

Baker, E.W., Louda, J.W., 1986. Porphyrins in the geological record. In: Johns, R.B. (Ed.), Biological Markers in the Sedimentary Record. Elsevier, Amsterdam, pp. 125–225.

Bhatia, M.R., Crook, K.A., 1986. Trace element characteristics of graywackes and tectonic setting discrimination of sedimentary basins. Contrib. Mineral. Petrol. 92 (2), 181–193. https://doi.org/10.1007/BF00375292.

Bjorøy, M., Vigran, J.O., 1980. Geochemical study of the organic matter in outcrop samples from Agardhfjellet. Spitsbergen. Phys. Chem. Earth. 12, 141–147. https://doi.org/10.1016/0079-1946(79)90096-X.

Bourbonniere, R.A., Meyers, P.A., 1996. Sedimentary geolipid records of historical changes in the watersheds and productivities of Lakes Ontario and Erie. Limnol. Oceanogr. 41, 352–359. https://doi.org/10.4319/lo.1996.41.2.0352.

Bray, E.E., Evans, E.D., 1961. Distribution of n-paraffins as a clue to recognition of source beds. Geochim. Cosmochim. Acta 22, 2–15. https://doi.org/10.1016/0016-7037(61)90069-2.

Brooks, P.W., Fowler, M.G., MacQueen, R.W., 1988. Biological marker conventional organic geochemistry of oilsands/heavy oils, Western Canada Basin. Org. Geochem. 12, 519–538. https://doi.org/10.1016/0146-6380(88)90144-1.

Brumsack, H.J., 2006. The trace metal content of recent organic carbon-rich sediments: implications for cretaceous black shale formation. Palaeogeogr. Palaeoclimatol. Palaeoecol. 232, 344–361. https://doi.org/10.1016/j.palaeo.2005.05.011.

Cañipa-Morales, N.K., Galán-Vidal, C.A., Guzmán-Vega, M.A., Jarvie, D.M., 2003. Effect of evaporation on C7 light hydrocarbon parameters. Org. Geochem. 34, 813–826. https://doi.org/10.1016/S0146-6380(03)00002-0.

Cao, J., Wu, M., Chen, Y., 2012. Trace and rare earth element geochemistry of Jurassic mudstones in the northern Qaidam Basin, Northwest China. Chem. Erde.: Geochem. 72 (3), 245–252. https://doi.org/10.1016/j.chemer.2011.12.002.

Cao, J., Yang, R., Hu, G., et al., 2018. Hydrocarbon potential of the lower cretaceous mudstones in coastal southeastern China. Am. Assoc. Pet. Geol. Bull. 102 (2), 333–366. https://doi.org/10.1306/0503171617917074.

Carvajal-Ortiz, H., Gentzis, T., 2015. Critical considerations when assessing hydrocarbon plays using Rock-Eval pyrolysis and organic petrology data: data quality revisited. Int. J. Coal Geol. 31st Annual Meeting of TSOP. 152, 113–122. https://doi.org/10.1016/j.coal.2015.06.001.

Cassani, F., Gallango, O., Talukdar, S., Vallejos, C., Ehrmann, U., 1988. Methylphenanthrene maturity index of marine source rock extracts and crude oils from the Maracaibo Basin. Org. Geochem. 73–80 https://doi.org/10.1016/B978-0-08-037236-5.50013-0.

Chen, L., Lu, Y., Jiang, S., Li, J., Guo, T., Luo, C., 2015. Heterogeneity of the lower Silurian Longmaxi marine shale in the Southeast Sichuan Basin of China. Mar. Pet. Geol. 65, 232–246. https://doi.org/10.1016/j.marpetgeo.2015.04.003.

Clayton, J.L., King, J.D., 1987. Effects of weathering on biological marker and aromatic hydrocarbon composition of organic matter in Phosphoria shale outcrop. Geochim. Cosmochim. Acta 51, 2153–2157. https://doi.org/10.1016/0016-7037(87)90264-X.

Clayton, J.L., Swetland, P.J., 1978. Subaerial weathering of sedimentary organic matter. Geochim. Cosmochim. Acta 42 (3), 305–312. https://doi.org/10.1016/0016-7037(78)90183-7.

Cockell, C.S., Pybus, D., Olsson-Francis, K., 2011. Molecular characterization and geological microenvironment of a microbial community inhabiting weathered receding shale cliffs. Microb. Ecol. 61, 166–181. https://doi.org/10.1007/s00248-010-9730-6.

Dai, J., Ni, Y., Qin, S., Huang, S., Peng, W., Han, W., 2018. Geochemical characteristics of ultra-deep natural gas in the Sichuan Basin, SW China. Pet. Explor. Dev. 45, 619–628. https://doi.org/10.1016/S1876-3804(18)30067-3.

Diskin, S., Evans, J., Fowler, M.B., Guion, P.D., 2011. Recognising different sediment provenances within a passive margin setting: Towards characterising a sediment source to the west of the British late Carboniferous sedimentary basins. Chem. Geol. 283 (3–4), 143–160. https://doi.org/10.1016/j.chemgeo.2010.10.007.

Duliu, O.G., Cristache, C.I., Culicovc, O.A., Frontasyeva, M.V., Szobotca, S.A., Toma, M., 2009. Epithermal neutron activation analysis investigation of Clarion–Clipperton abyssal plane clay and polymetallic micronodules. Appl. Radiat. Isot. 67 (5), 939–943. https://doi.org/10.1016/j.apradiso.2009.01.062.

Eastcott, L., Shiu, W.Y., Mackay, D., 1988. Environmentally relevant physical-chemical properties of hydrocarbons: A review of data and development of simple correlations. Oil Chem. Pollut. 4, 191–216. https://doi.org/10.1016/S0269-8579(88)80020-0.

Fan, Z.Q., Jin, Z.H., Johnson, S.E., 2012. Modelling petroleum migration through microcrack propagation in transversely isotropic source rocks. Geophys. J. Int. 190 (1), 179–187. https://doi.org/10.1111/j.1365-246X.2012.05516.x.

Fathi, E., Akkutlu, I.Y., 2009. Matrix heterogeneity effects on gas transport and adsorption in coalbed and shale gas reservoirs. Transp. Porous Media 80 (2), 281–304. https://doi.org/10.1007/s11242-009-9359-4.

Faure, P., Landais, P., Griffault, L., 1999. Behavior of organic matter from Callovian shales during low-temperature air oxidation. Fuel. 78, 1515–1525. https://doi.org/10.1016/S0016-2361(99)00086-1.

Fedo, C.M., Wayne Nesbitt, H., Young, G.M., 1995. Unraveling the effects of potassium metasomatism in sedimentary rocks and paleosols, with implications for paleoweathering conditions and provenance. Geology 23, 921–924. https://doi.org/10.1130/0091-7613(1995)023<0921:UTEOPM>2.3.CO;2.

Fischer, C., Schmidt, C., Bauer, A., Gaupp, R., Heide, K., 2009. Mineralogical and geochemical alteration of low-grade metamorphic black slates due to oxidative weathering. Geochemistry 69, 127–142. https://doi.org/10.1016/j.chemer.2009.02.002.

Frings, P.J., Buss, H.L., 2019. The central role of weathering in the geosciences. Elements. 15 (4), 229–234. https://doi.org/10.2138/gselements.15.4.229.

Gieskes, J.M., Simoneit, B.R.T., Magenheim, A.J., Leif, R.N., 1990. Retrograde oxidation of hydrothermal precipitates and petroleum in Escanaba Trough sediments. Appl. Geochem. 5 (1–2), 93–101. https://doi.org/10.1016/0883-2927(90)90040-C.

Glattke, T.J., Chacón-Patiño, M.L., Marshall, A.G., Rodgers, R.P., 2020. Molecular characterization of photochemically produced asphaltenes via photooxidation of deasphalted crude oils. Energy Fuel 34, 14419–14428. https://doi.org/10.1021/acs.energyfuels.0c02654.

Goklen, K.E., Stoecker, T.J., Baddour, R.F., 1984. A method for the isolation of Kerogen from green river oil-shale. Ind. Eng. Chem. Prod. Res. Dev. 23 (2), 308–311. https://doi.org/10.1021/i300014a028.

Han, S., Hong, J., Luo, Q., Xu, H., Tan, H., Wang, Q., Tao, J., Zhou, Y., Peng, L., He, Y., Shi, J., Ma, N., Cheng, Y., Su, H., 2022. Hygroscopicity of organic compounds as a function of organic functionality, water solubility, molecular weight, and oxidation level. Atmos. Chem. Phys. 22, 3985–4004. https://doi.org/10.5194/acp-22-3985-2022.

Hannigan, R.E., Sholkovitz, E.R., 2001. The development of middle rare earth element enrichments in freshwaters: weathering of phosphate minerals. Chem. Geol. 175, 495–508. https://doi.org/10.1016/S0009-2541(00)00355-7.

Harnois, L., 1988. The CIW index: a new chemical index of weathering. Sediment. Geol. 55, 319–322. https://doi.org/10.1016/0037-0738(88)90137-6.

Haskin, L.A., Haskin, M.A., Frey, F.A., Wilderman, T.R., 1968. Relative and absolute terrestrial abundances of the rare earths. In: Ahrens, L.H. (Ed.), Origin and Distribution of the Elements. Pergamon, Oxford, pp. 889–912. https://doi.org/10.1016/B978-0-08-012835-1.50074-X.

Hatch, J.R., Leventhal, J.S., 1992. Relationship between inferred redox potential of the depositional environment and geochemistry of the Upper Pennsylvanian (Missourian) Stark Shale Member of the Dennis Limestone, Wabaunsee County, Kansas, USA. Chem. Geol. 99, 65–82. https://doi.org/10.1016/0009-2541(92)90031-Y.

Jiang, C., Chen, Z., Mort, A., Milovic, M., Robinson, R., Stewart, R., Lavoie, D., 2016. Hydrocarbon evaporative loss from shale core samples as revealed by Rock-Eval and thermal desorption-gas chromatography analysis: its geochemical and geological

implications. Mar. Pet. Geol. 70, 294–303. https://doi.org/10.1016/j.marpetgeo.2015.11.021.
Jin, L., Ma, L., Dere, A., White, T., Mathur, R., Brantley, S.L., 2017. REE mobility and fractionation during shale weathering along a climate gradient. Chem. Geol. 466, 352–379. https://doi.org/10.1016/j.chemgeo.2017.06.024.
Jones, B., Manning, D.A.C., 1994. Comparison of geochemical indices used for the interpretation of palaeoredox conditions in ancient mudstone. Chem. Geol. 111, 111–129. https://doi.org/10.1016/0009-2541(94)90085-X.
Kolowith, L.C., Berner, R.A., 2002. Weathering of phosphorus in black shales. Glob. Biogeochem. Cycles 16. https://doi.org/10.1029/2001GB001887 (issn: 0886–6236).
Krzeszowska, E., 2019. Geochemistry of the Lublin Formation from the Lublin Coal Basin: Implications for weathering intensity, palaeoclimate and provenance. Int. J. Coal Geol. 216, 103306 https://doi.org/10.1016/j.coal.2019.103306.
Lafargue, E., Barker, C., 1988. Effect of water washing on crude oil compositions. Am. Assoc. Pet. Geol. Bull. 72 (3), 263–276. https://doi.org/10.1306/703C8C13-1707-11D7-8645000102C1865D.
Leythaeuser, D., 1973. Effects of weathering on organic matter in shales. Geochim. Cosmochim. Acta 37 (1), 113–120. https://doi.org/10.1016/0016-7037(73)90249-4.
Li, D., Li, R., Wang, B., Liu, Z., Wu, X., Liu, F., 2016. Study on oil-source correlation by analyzing organic geochemistry characteristics: a case study of the Upper Triassic Yanchang Formation in the south of Ordos Basin, China. Acta Geochim. 35 (4), 1–13. https://doi.org/10.1007/s11631-016-0123-5.
Li, D., Li, R., Zhu, Z., Wu, X., Cheng, J., Liu, F., Zhao, B., 2017. Origin of organic matter and paleo-sedimentary environment reconstruction of the Triassic oil shale in Tongchuan City, southern Ordos Basin (China). Fuel. 208, 223–235. https://doi.org/10.1016/j.fuel.2017.07.008.
Li, J., Tao, X., Bai, B., Huang, S., Jiang, Q., Zhao, Z., Chen, Y., Ma, D., Zhang, L., Li, N., Song, W., 2021. Geological conditions, reservoir evolution and favorable exploration directions of marine ultra-deep oil and gas in China. Pet. Explor. Dev. 48, 60–79. https://doi.org/10.1016/S1876-3804(21)60005-8.
Liao, Y., Geng, A., Huang, H., 2009. The influence of biodegradation on resins and asphaltenes in the Liaohe Basin. Org. Geochem. 40, 312–320. https://doi.org/10.1016/j.orggeochem.2008.12.006.
Littke, R., Klussmann, U., Krooss, B., Leythaeuser, D., 1991. Quantification of loss of calcite, pyrite, and organic matter due to weathering of Toarcian black shales and effects on kerogen and bitumen characteristics. Geochim. Cosmochim. Acta 55 (11), 3369–3378. https://doi.org/10.1016/0016-7037(91)90494-P.
Liu, W., Liao, Y., Jiang, C., Pan, Y., Huang, Y., Wang, X., Wang, Y., Peng, P., 2022. Superimposed secondary alteration of oil reservoirs. Part II: the characteristics of biomarkers under the superimposed influences of biodegradation and thermal alteration. Fuel. 307, 121721 https://doi.org/10.1016/j.fuel.2021.121721.
Liu, W., Liao, Y., Pan, Y., Jiang, B., Zeng, Q., Shi, Q., Hsu, C.S., 2018. Use of ESI FT–ICR MS to investigate molecular transformation in simulated aerobic biodegradation of a sulfur-rich crude oil. Org. Geochem. 123, 17–26, 10/gd4m26.
Ma, L., Jin, L., Brantley, S.L., 2011. How mineralogy and slope aspect affect REE release and fractionation during shale weathering in the Susquehanna/Shale Hills critical Zone Observatory. Chem. Geol. 290, 31–49. https://doi.org/10.1016/j.chemgeo.2011.08.013.
Mackenzie, A.S., McKenzie, D.P., 1983. Aromatization and isomerization of hydrocarbons in sedimentary basins formed by extension. Geol. Mag. 120, 417–470. https://doi.org/10.1017/S0016756800027461.
Marynowski, L., Wyszomirski, P., 2008. Organic geochemical evidences of early diagenetic oxidation of the terrestrial organic matter during the Triassic arid and semi-arid climatic conditions. Appl. Geochem. 23, 2612–2618. https://doi.org/10.1016/j.apgeochem.2008.05.011.
Marynowski, L., Kurkiewicz, S., Rakociński, M., Simoneit, B.R., 2011a. Effects of weathering on organic matter: I. changes in molecular composition of extractable organic compounds caused by paleoweathering of a lower Carboniferous (Tournaisian) marine black shale. Chem. Geol. 285 (1–4), 144–156. https://doi.org/10.1016/j.chemgeo.2011.04.001.
Marynowski, L., Szełęg, E., Jędrysek, M.O., Simoneit, B.R., 2011b. Effects of weathering on organic matter: Part II: Fossil wood weathering and implications for organic geochemical and petrographic studies. Org. Geochem. 42 (9), 1076–1088. https://doi.org/10.1016/j.orggeochem.2011.06.017.
Marynowski, L., Pisarzowska, A., Derkowski, A., Rakociński, M., Szaniawski, R., Środoń, J., Cohen, A.S., 2017. Influence of palaeoweathering on trace metal concentrations and environmental proxies in black shales. Palaeogeogr. Palaeoclimatol. Palaeoecol. 472, 177–191. https://doi.org/10.1016/j.palaeo.2017.02.023.
McArthur, J.M., Walsh, J.N., 1984. Rare-earth geochemistry of phosphorites. Chem. Geol. 47, 191–220. https://doi.org/10.1016/0009-2541(84)90126-8.
McAuliffe, C.D., 1979. Chemical and physical constraints on petroleum migration with emphasis on hydrocarbon solubilities in water. In: Roberts III, W.H., Cordell, R.J. (Eds.), Physical and chemical constraints on petroleum migration: AAPG Continuing Education Source Notes Series 8. https://doi.org/10.1306/CE8396C3. C-1 to C-39.
Meng, Y., Xiao, L., Yang, J., 1999. Influences of weathering on organic matter of outcrop andcorrecting methods in Xining basin. Geochimica 28 (1), 42–50 (in Chinese with English abstract).
Nesbitt, H.W., Young, G.M., 1982. Early proterozoic climates and plate motions inferred from major element chemistry of lutites. Nature 299 (5885), 715–717. https://doi.org/10.1038/299715a0.
Palmer, S.E., 1984. Effect of Water Washing on C_{15+} Hydrocarbon Fraction of crude oils from Northwest Palawan, Philippines1. Am. Assoc. Pet. Geol. Bull. 68, 137–149. https://doi.org/10.1306/AD4609EA-16F7-11D7-8645000102C1865D.
Palmer, S.E., 1993. Effect of biodegradation and water washing on crude oil composition. Org. Geochem.: Principles and Applications, Topics in Geobiology 511–533. https://doi.org/10.1007/978-1-4615-2890-6_23.
Pan, S., Jiang, Z., Zhang, Y., Yuan, X., Liao, Y., 2021. Geochemical characteristics of the lower cretaceous Xiguayuan Formation mudrocks in the Luanping Basin, northern China: Implications for the hydrocarbon generation potential and sedimentary environments. Mar. Pet. Geol. 133, 105256 https://doi.org/10.1016/j.marpetgeo.2021.105256.
Pan, Y., Liao, Y., Shi, Q., 2017. Variations of Acidic Compounds in Crude Oil during Simulated Aerobic Biodegradation: Monitored by Semiquantitative Negative-Ion ESI FT-ICR MS. Energy Fuels 31, 1126–1135, 10/f9w494.
Panahi, A., Young, G.M., Rainbird, R.H., 2000. Behavior of major and trace elements (including REE) during Paleoproterozoic pedogenesis and diagenetic alteration of an Archean granite near Ville Marie, Quebec. Canada. Geochim. Cosmochim. Acta. 64 (13), 2199–2220. https://doi.org/10.1016/S0016-7037(99)00420-2.
Peters, K.E., Moldowan, J.M., 1993. The Biomarker Guide, 1st edition. Prentice Hall, New York.
Peters, K.E., Walters, C.C., Moldowan, J.M., 2005. The Biomarker Guide, Biomarkers and Isotopes in Petroleum Exploration and Earth History, 2nd ed. Cambridge University Press, New York, NY.
Petsch, S.T., Berner, R.A., Eglinton, T.I., 1999. Organic matter loss and alteration during black shale weathering. In: Armannsson, Halldor (Ed.), Geochemistry of the Earth's Surface: Proceedings of the 5th International Symposium. CRC Press, Rotterdam, pp. 271–274. Reykjavik, 16–20, August 1999.
Petsch, S.T., Berner, R.A., Eglinton, T.I., 2000. A field study of the chemical weathering of ancient sedimentary organic matter. Org. Geochem. 31 (5), 475–487. https://doi.org/10.1016/S0146-6380(00)00014-0.
Petsch, S.T., Smernik, R.J., Eglinton, T.I., Oades, J.M., 2001. A solid state 13C-NMR study of kerogen degradation during black shale weathering. Geochim. Cosmochim. Acta 65 (12), 1867–1882. https://doi.org/10.1016/S0016-7037(01)00572-5.
Petsch, S.T., Edwards, K.J., Eglinton, T.I., 2005. Microbial transformations of organic matter in black shales and implications for global biogeochemical cycles. Palaeogeogr. Palaeoclimatol. Palaeoecol. 219 (1–2), 157–170. https://doi.org/10.1016/j.palaeo.2004.10.019.
Peucker-Ehrenbrink, B., Hannigan, R.E., 2000. Effects of black shale weathering on the mobility of rhenium and platinum group elements. Geology 28, 475–478. https://doi.org/10.1130/0091-7613(2000)28<475:EOBSWO>2.0.CO;2.
Price, L.C., 1976. Aqueous solubility of petroleum as applied to its origin and primary migration: Am. Assoc. Pet. Geol. Bull. 60, 213–244. https://doi.org/10.1306/83D922A8-16C7-11D7-8645000102C1865D.
Qiao, J., Littke, R., Grohmann, S., Zhang, C., Jiang, Z., Strauss, H., Zieger, L., 2022. Climatic and environmental conditions during the Pleistocene in the Central Qaidam Basin, NE Tibetan Plateau: evidence from GDGTs, stable isotopes and major and trace elements of the Qigequan Formation. Int. J. Coal Geol. 254, 103958 https://doi.org/10.1016/j.coal.2022.103958.
Qin, J., Wang, S., Sanei, H., Jiang, C., Chen, Z., Ren, S., Xu, X., Yang, J., Zhong, N., 2018. Revelation of organic matter sources and sedimentary environment characteristics for shale gas formation by petrographic analysis of middle Jurassic Dameigou formation, northern Qaidam Basin, China. Int. J. Coal Geol. 195, 373–385. https://doi.org/10.1016/j.coal.2018.06.015.
Radke, M., 1988. Application of aromatic compounds as maturity indicators in source rocks and crude oils. Mar. Pet. Geol. 5, 224–236. https://doi.org/10.1016/0264-8172(88)90003-7.
Radke, M., Welte, D.H., 1983. The Methylphenanthrene Index (MPI). A maturity parameter based on aromatic hydrocarbons. In: Bjorøy, M., et al. (Eds.), Advances in Organic Geochemistry. J. Wiley and Sons, New York, pp. 504–512.
Ramos, C.E., 2015. Geochemical source rock evaluation in the Lusitanian Basin (Portugal) using TG/DSC analysis. In: A Master Thesis of Science Degree in Energy Engineering and Management, Portuguese School of Engineering. Science and Technology, the Technical University of Lisbon, Portugal.
Sageman, B.B., Lyons, T.W., 2003. Geochemistry of fine-grained sediments and sedimentary rocks. Treatise Geochem. 7, 407. https://doi.org/10.1016/B0-08-043751-6/07157-7.
Scalan, E.S., Smith, J.E., 1970. An improved measure of the odd-even predominance in the normal alkanes of sediment extracts and petroleum. Geochim. Cosmochim. Acta 34, 611–620. https://doi.org/10.1016/0016-7037(70)90019-0.
Seifert, W.K., Moldowan, J.M., 1979. The effect of biodegradation on steranes and terpanes in crude oils. Geochim. Cosmochim. Acta 43 (1), 111–126. https://doi.org/10.1016/0016-7037(79)90051-6.
Seifert, W.K., Moldowan, J.M., 1986. Use of biological markers in petroleum exploration. Methods Geochem. Geophys. 24, 261–290.
Skręt, U., Fabiańska, M.J., Misz-Kennan, M., 2010. Simulated water-washing of organic compounds from self-heated coal wastes of the Rymer Cones Dump (Upper Silesia Coal Region, Poland). Org. Geochem. 41, 1009–1012. https://doi.org/10.1016/j.orggeochem.2010.04.010.
Song, S.J., Liu, Y.Q., Zheng, Q.H., Zhou, D.W., Fu, Y., 2019. Genesis analysis of black rock series: a case study of Chang 7-3 member in Tongchuan area. Acta Sedimentol. Sin. 37 (6), 1117–1128.
Spears, D.A., Taylor, R.K., 1972. The influence of weathering on the composition and engineering properties of in situ coal measures rocks. Int. J. Rock Mech. Min. Sci. Geomech. Abstr. 9 (6), 729–730. https://doi.org/10.1016/0148-9062(72)90033-2.
Tamamura, S., Ueno, A., Aramaki, N., Matsumoto, H., Uchida, K., Igarashi, T., Kaneko, K., 2015. Effects of oxidative weathering on the composition of organic matter in coal and sedimentary rock. Org. Geochem. 81, 8–19. https://doi.org/10.1016/j.orggeochem.2015.01.006.

Tang, X., Zhang, J., Liu, Y., Yang, C., Chen, Q., Dang, W., Zhao, P., 2018. Geochemistry of organic matter and elements of black shale during weathering in northern Guizhou, southwestern China: their mobilization and inter-connection. Geochemistry. 78, 140–151. https://doi.org/10.1016/j.chemer.2017.08.002.

Tao, G.L., Shen, B.J., Boltsjin, T., Yang, Y., Xu, E.S., Pan, A.Y., 2016. Weathering effects on high-maturity organic matter in a black rock series: a case study of the Yuertusi Formation in Kalpin area, Tarim Basin. Pet. Geol. Exp. 38 (3), 375–381 (in Chinese with English abstract).

Taylor, S.R., McLennan, S.M., 1985. The Continental Crust: Its Composition and Evolution. Blackwell Scientific Publications Ltd, Palo Alto, CA, p. 312.

Tuttle, M.L.W., Breit, G.N., Goldhaber, M.B., 2009. Weathering of the New Albany Shale, Kentucky: II. Redistribution of minor and trace elements. Appl. Geochem. 24, 1565–1578. https://doi.org/10.1016/j.apgeochem.2009.04.034.

Tuttle, M.L.W., Fahy, J.W., Elliott, J.G., Grauch, R.I., Stillings, L.L., 2014. Contaminants from cretaceous black shale: I. Natural weathering processes controlling contaminant cycling in Mancos Shale, southwestern United States, with emphasis on salinity and selenium. Appl. Geochem. 46, 57–71. https://doi.org/10.1016/j.apgeochem.2013.12.010.

Volkman, J.K., Alexander, B., Kagi, R.I., Woodhouse, G.W., 1983. Demethylated hopanes in crude oils and their application in petroleum geochemistry. Geochim. Cosmochim. Acta 47, 785–794. https://doi.org/10.1016/0016-7037(83)90112-6.

Wardroper, A.M.K., Hoffmann, C.F., Maxwell, J.R., Barwise, A.J.G., Goodwin, N.S., Park, P.J.D., 1984. Crude oil biodegradation under simulated and natural conditions—II. Aromatic steroid hydrocarbons. Org. Geochem. 6, 605–617. https://doi.org/10.1016/0146-6380(84)90083-4.

Wedepohl, K.H., 1995. The composition of the continental crust. Geochim. Cosmochim. Acta 59, 1217–1232. https://doi.org/10.1016/0016-7037(95)00038-2.

Wei, J.S., Lu, J.C., Wei, X.Y., Han, W., Jiang, T., 2012. The influence of intense weathering on the evaluation indexes of hydrocarbon source rocks: a case study of Carboniferous-Permian Strata of Ejin Banner and its neighboring areas. Geol. Bull. China. 31 (10), 1715–1723 (in Chinese with English abstract).

Wignall, P.B., 1994. Black Shales, vol. 127. Clarendon Press, Oxford.

Wildman, R.A., Berner, R.A., Petsch, S.T., Bolton, E.W., Eckert, J.O., Mok, U., Evans, J.B., 2004. The weathering of sedimentary organic matter as a control on atmospheric O2: I. Analysis of black shale. Am. J. Sci. 304 (3), 234–249. https://doi.org/10.2475/ajs.304.3.234.

Wright, J., Schrader, H., Holser, W.T., 1987. Paleoredox variations in ancient oceans recorded by rare earth elements in fossil apatite. Geochim. Cosmochim. Acta 51 (3), 631–644. https://doi.org/10.1016/0016-7037(87)90075-5.

Wu, X.Y., Ling, S.X., Ren, Y., 2016. Elemental migration characteristics and chemical weathering degree of black shale in Northeast Chongqing China. Earth Sci. 41 (2), 218–233 (in Chinese with English abstract).

Zhang, K., Liu, R., Ding, W., Li, L., Liu, Z., 2022. The influence of early cretaceous paleoclimate warming event on sedimentary environment evolution and organic matter sources in Yin'e Basin: evidence from petrology and molecular geochemistry. Int. J. Coal Geol. 254, 103972 https://doi.org/10.1016/j.coal.2022.103972.

Zheng, Y., Liao, Y., Wang, Y., Xiong, Y., Xiong, Y., 2018. Organic geochemical characteristics, mineralogy, petrophysical properties, and shale gas prospects of the Wufeng–Longmaxi shales in Sanquan Town of the Nanchuan District, Chongqing. Am. Assoc. Pet. Geol. Bull. 102 (11), 2239–2265. https://doi.org/10.1306/04241817065.